1-1-2014

Novel Nanocomposite Material For Supercapacitor Applications

Wissam Fawaz
Wayne State University,

NOVEL NANOCOMPOSITE MATERIAL FOR SUPERCAPACITOR APPLICATIONS

By

WISSAM FAWAZ

THESIS

Submitted to the Graduate School

of Wayne State University

in partial fulfillment of the requirements

for the degree of

MASTER OF SCIENCE

2014

Major: PHYSICS

Approved by:

_____

Advisor: Date:

DEDICATION

"To Professor Gavin Lawes"

It was your belief in me that drove me towards graduate studies; none of this would be possible without you. Thank you.

ACKNOWLEDGMENTS

Many people deserve acknowledgment for the completion of this thesis, but none more than my advisors Professor Ratna Naik and Professor Gholam Abbas Nazri. Their continuous support and encouragement helped me surmount the miscellaneous hurdles on the path to bring my research to fruition in the form of this work. Through the cacophony of time consuming academic pursuits and parental duties, Professor Naik's boundless patience eased the burden, her immeasurable grace propelled me forward, and soundness of vision kept on an accurate academic track. Professor Nazri on the other hand, is the model scientist that we all wish to emulate: An ever flowing river of knowledge matched only by his quick wit and cheerful spirit, and an unmatched passion for research.

Thanks should also be extended to Professor Gavin Lawes, Professor Sean Gavin, and Dr Balaji Mandal for their encouragement, advice and honest friendship, Professor Zhixian Zhou for academic and research assistance and beneficial conversations.

The completion of this work would not have been possible without the marvelous cooperation and friendships that I encountered throughout my graduate studies at the Physics department. Without limiting anyone's role, I would like to thank Dr Ambesh Dixit, Dr Alan Sebastian, Dr Khadija Bazzi, Laura Gunther, Suvra Laha, Rupam Mukherjee, and Kurt Van Delinder for help and guidance inside and outside the lab setting.

I would also like to extend a special recognition to Joydeep Roy, Karen Burke, Humeshkar Nemala, Ajay Kumar, Kulwinder Dhindsa, and Ehab Abd Elhamid. The friendships I have forged with each of them made us as close as family, and helped me my arduous task.

Preface

In the age when the electrification of transportation is no longer a distant dream, the need for advanced energy storage is more crucial than ever. Supercapacitors are among the most sought after devices for the storage of electrical charge. Its simple, effective, stable and eco-friendly design has propelled it to the top researched areas in electrochemistry, and it is widely believed to be the last corner stone in vehicle electrification. The supercapacitor enjoys a rapid charge-discharge time, an extensive cycle life, inexpensive and light parts, and able to deliver a sweeping amount of power in short bursts. This is why numerous researches are geared towards coupling the supercapacitor with lithium batteries, since the latter is endowed with a wide energy density whilst supercapacitors boast a superb power density.

In the present work, we introduce the technology's history and current status, its working mechanisms and working milieus, as well as its future trends. Chapters 4 and 5 of this thesis present work done on material for a pseudocapacitor: The material preparation and characterization are shown in chapter 4 and its electrochemical performance is studied in chapter 5.

This thesis also includes a modeling appendix to further emphasis the performance advancement in hybrid electric vehicles, with the tethering of a supercapacitor bank to the on-board energy storage.

List of Figures

TABLE OF CONTENTS

Chapter 1

Introduction

The energy storage systems are crucial part of any energy strategy, and supercapacitors are one of the most efficient energy storage devices with very high power capability. The global market share of supercapacitors is rapidly growing, and newer models have higher energy density than their predecessors. Current primary energy sources such as fossil fuels (Gas, Oil and Coal) are limited and will not likely be easily available past 2042[1]. Energy is crucial for the sustainability of modern societies; it is the economic backbone of any sustainable social construct. Recently geopolitical conflicts as well as the constant rise in the price of fuel, the continuous rise in world population and modernization of societies, the wide spread use of portable electronics, power tools and electric-based transportation have created a sharp increase in consumption of energy sources.[2] Currently, less than 20% of the world's energy demands are being met by renewables and nuclear power, and the efficiency of converting these alternative energy sources to electricity is not as high as that of fossil fuels.

Carbon-based resources are basis of the worldwide energy economy, and have been for the last two centuries. The world started feeling the impact of this long term dependence on fossil fuels, and the increase in public awareness of the dangers that

NOx, SOx and other greenhouse gases that are being released into the atmosphere from combustion processes, drove several nations to sign the famous Kyoto protocol and commit to hard challenges to curb global warming[3]. On the other hand, solar, geothermal, Biomass and wind power energies are abundant and underused. The cost of energy from these sources is continuously coming down whilst the cost to extract energy from fossil fuels is on the rise. Creating a grid and developing these energy source are the world's greatest challenges for this century[4]. Unfortunately most of the alternative energies such as solar and wind are intermittent. To deal with their intermittency, energy storage devices are needed. Among various energy storage systems, the electrochemical systems are the most efficient for storing energy and releasing energy on demand at ambient and sub-ambient temperatures. Advanced batteries have made significant progress during last two decades, and lithium-ion battery is dominating the field. However, the power capability of the lithium battery is limited to the rate of ion diffusion in solid electrodes. There is an urgent need to develop high power energy storage device, and supercapacitors are the most desirable sources for high rate high power applications. New portable electronics require portable energy sources that could handle various power peak demands. Current lithium batteries are facing a challenge to provide the necessary requirements for powering the electric based transportation and for future electronics[5].

Transportation sectors currently use over 60% of the world's production of oil, and are also contributing the most to the increase in greenhouse gases. Rising

awareness of environmental concerns as well as the unsustainability in current oil supply model is prompting auto makers to intensify their search for environmentally friendly and more energy efficient vehicles. Almost every automotive company has rolled out several HEV and EV models. In recent years, more automakers[6] are making use of the supercapacitor's ability to deliver very high charge/discharge cycles, to meet the power requirements of newer HEVs and EVs[7]. Peak power sizing of the battery pack aboard the electric vehicle greatly affects the requirement for size and weight of the energy storage system. The battery pack is required to deliver power surges needed for grade climbing and acceleration, while accepting transient power through regenerative breaking[8]. These wildly varying current surges generate heat inside the battery, and lead to premature failure of the battery pack, especially when the battery is near its full state of charge (SOC). Using a supercapacitor relieves the battery peak power stress and it seems to have become a crucial part in vehicle electrification[7, 8]. Hybridization of battery and supercapacitor is also an ideal energy management for buses and fleets operations. Schematic of battery and supercapacitor hybridization is shown in Figure 1. With this novel approach to the electrification of the automobile, several designs have been proposed to couple the battery and a supercapacitor in numerous HEV and EV models[9]. Figure 2 present one such design with a variable primary energy source (i.e. gasoline or fuel cells or batteries). The role of the inverter is to deliver energy from the battery pack into the motor on demand and reversibly input the charge back into the supercapacitor upon regenerative braking.

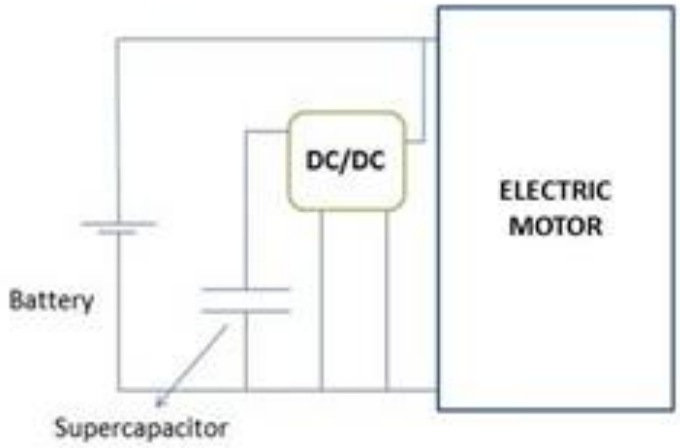

Figure 1. Illustraction of battery – supercapacitor hybrid for electrification of automobile. The battery and the supercapacitor are using convertors to adjust their voltages for the application.

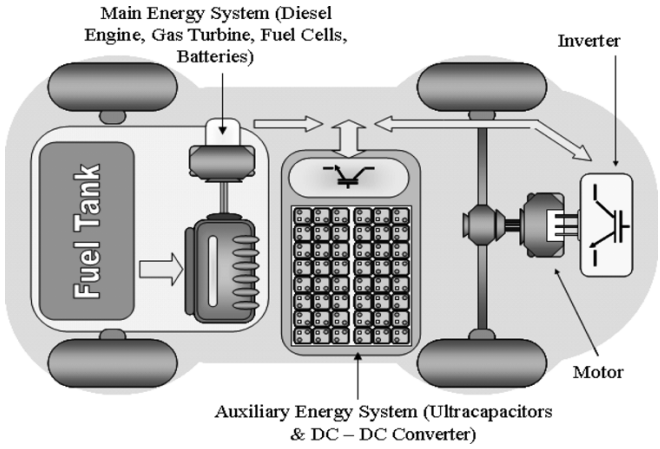

Figure 2. A general perspective of hybrid electric vehicle components, a small ICE, hybrid of battery – supercapacitor, convertors-invertors and electric motor[10].

1.1 Current and Future Status of Supercapacitors

While capacitors have been in use for more than a century, they have not been known to hold much charge, and their use was mainly to compliment circuits or memory storage devices. In 1957, G.E. patented a device made of porous carbon which showed promise in holding high capacitance. SOHIO patented another device in 1966 and explicitly explained how the energy is stored at the carbon pores, with the electrode/electrolyte double-layer interfaces acting as capacitors. The sales of the device were limited, and SOHIO sold the patent to NEC (NIPPON ELECTRIC COMPANY). NEC coined the term SUPERCAPACITOR and its successful model finally pushed these devices into commercial use in memory backups and home appliances. Other examples followed such as Dynacap and PRI, and were able to establish supercapacitors as high power energy storage devices. By the end of 1992 the United States Department of Energy (DOE) had already a supercapacitor program being run at Maxwell labs. Various companies have their own system available on the market and many more actively involved in research and development of supercapacitor materials.

Another avenue of interest for supercapacitor research is flexible energy storage devices. The malleability of most carbonaceous material suitable for supercapacitor electrodes, such as free standing graphene oxide films, makes them attractive as electrodes, or as a conductive base to grow metal oxides for pseudocapacitive effects[11]. The excellent conductivity and mechanical properties of these electrodes makes them

attractive for the area of flexible high power electronics[12], as well as textile energy storage devices. These “wearable” energy storage systems could provide power to medical monitoring devices, illumination, as well as an array of consumer electronics[13].

Chapter 2

Principles of Operation of Supercapacitors

The supercapacitor stores energy in three ways:

a) In the electric field of the interfacial double layer of the electrode/electrolyte interfaces. This is referred to as the double layered capacitance originally thought out by Hermann Von Helmholtz. This is an entirely non-faradaic process which does not involve any making or breaking of chemical bonds [14], but rather charges are stored in the electric field formed between electrons on the surface of the electrode and ions in the electrolyte that are adsorbed at the electrode surface. Helmholtz's model fell short is describing the multitude of processes happening at the electrode/electrolyte interface. Gouy and Chapman presented a model of the double layer effect that accounts for the diffusion of the ions in the electrolyte called a diffusion layer then Stern combined both models and presented a more complete model coined as stern layer.

b) Through electrosorption and surface redox reactions (pseudocapacitance) on p-doped or n-doped electrodes, which have been reported to match and sometimes exceed the performance of EDLC[15]. The type of reactions happening at the surface is faradaic in nature in the sense that the charge transfer is voltage dependent, as shown in the following Nernst equation (1) which relates the half-cell reactions to its standard potential and concentration of the species: E^0 is the standard potential, R is the gas

constant, *T* is the absolute temperature, *F* is the Faraday constant, and $\mathfrak{R}$ is defined as the concentration of oxidants divided by the concentration of the reductant.

$$E = E^0 - \frac{RT}{zF} ln\ (\mathfrak{R}) \qquad (1)$$

Z is the amount of charge. Pseudocapacitance occurs due to adsorption/desorption of ions on the surface as well: A monolayer of ions gets deposited on the surface of the electrode which gives rise to faradaic reactions:

$$I^{+/-} \pm e^- \leftrightarrow I.A_{ads}$$

Where I is the concentration of depositable ionic species, A_{ads} is the surface area available for adsorption at some cell potential V.

c) By utilizing both the faradaic electrode and non-faradaic electrode processes, in what is known as the "Hybrid" capacitor[16]. This is a recent advancement to research on supercapacitors and yet at infancy. It aims to integrate the advantages of both Lithium Ion Batteries and the double layer effect of the traditional supercapacitor. The attractiveness of such an energy storage device is its high energy density coming from the battery – like anode as well as the non-faradaic high power density coming from the carbonaceous cathode. In other words, adsorption/desorption of anions occur at the surface of the cathode, whilst lithium ions are being inserted/extracted on the anodic side[17].

2.1 The double layered supercapacitor.

As shown in Figure 3 below, the construction of a supercapacitor includes a separator soaked in electrolyte, sandwiched between two high surface area electrodes usually made from activated carbon [18,19].

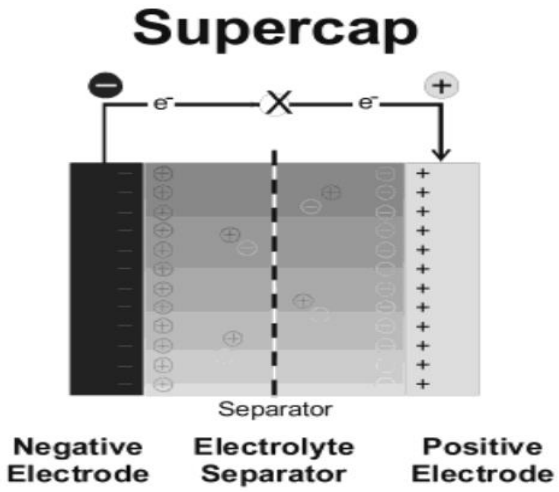

Figure 3 – Basic construction of a double layered Supercapacitor.

The capacitance of an EDLC follows the equation

$$C = \frac{\epsilon . A}{d} \qquad (2)$$

Where ϵ is the relative dielectric constant, A is the electrode surface area, and d is electrodes separation distance[20]. In order to enhance energy storage capacity of a capacitor, its surface area must be maximized and the electrode separation minimized. In addition the energy (E) of a capacitor is related to the square of its voltage (V) and its capacitance (C) through the following equation

$$E = \left(\frac{1}{2}\right) CV^2 \qquad (3)$$

Therefore increasing capacitor voltage is one of the main approaches to enhance energy density of the capacitors, this is why recently researchers are leaning towards the use of organic electrolytes which benefit from a wide voltage window.

Studies have already shown that porous carbon electrodes could have a surface area upwards of 2000 m^2 per gram. This type of capacitors is well researched in laboratories since the 1980s; it can withstand an applied voltage between -0.5 V and 1 V in an aqueous electrolyte. Further increase in the applied voltage may result in breaking down of the electrolyte (the electrochemical stability for water is about 1.23 V) or in irreversible polarization of the carbon electrode into CO_2 and any increase on the negative side might result in hydrogen evolution. The realistic capacitance of EDLCs made with porous carbon material such as activated carbon (AC), activated charcoal, carbon cloth and such is limited to about 100 $F.g^{-1}$. Such a limited specific capacitance has been attributed to pore sizes being too small for the ions to pass through, and the electrolyte is believed not to be in direct contact with the entire surface area of the carbon electrode[21-23].

Activated carbons were the first and most widely used material for EDLCs. Their high surface area (around 500 m^2 per gram) is due to the large number of micro-pores which riddle its surface. The most common activation method for this carbon is

chemical, through the use of acids or a strong base to create the pores needed to enlarge the surface area, followed by pyrolysis[24, 25]. The reported capacitance ranges from 63 to 100 $F.g^{-1}$ [26]. The same could be applied to activated carbon fibers, which benefit from slightly higher surface area than AC, but does not exhibit much larger capacitive behavior, which has been attributed to its low bulk density[23]. Carbon nano-fibers have been employed to increase tensile strength in many composites, and when activated, used as electrodes for Lithium batteries. However the reported specific capacitance is not very encouraging as possible electrodes for supercapacitors (1 to 60 $F.g^{-1}$)[27].

Templated mesoporous carbons were thought of as possible electrodes for double-layered capacitors, as they contains extended micro-pores allowing a better wetting of the interface area with the electrolyte[28]. Template mesoporous carbon is produced by allowing carbon material in the liquid phase to enter the well-controlled pores of a silica substrate: When the carbonation process is over, the pores that are formed in the carbonaceous material are well connected. However, template carbons exhibit a wide range of specific capacitance due to the pore size distribution, which is usually attributed to the varying nature of the precursor involved [29]. Capacitance values ranged from 89 $F.g^{-1}$ to 160 $F.g^{-1}$ depending on the electrolyte[30].

Carbon nanotubes are another candidate electrode material for supercapacitor. They are long hollow tubes with walls made from single sheet graphene. This of course

allows CNTS to enjoy high conductivity, coupled with a large exposed area. Unlike other carbonaceous sheets, CNTs suffer from no edge effect or decomposition of the electrolyte at higher potentials[31].

These advantageous effects make CNTs an ideal material for supercapacitors, but the bundling of the fibers together due to Van der Waals forces prevents wetting of the entire surface area and therefore limit the capacitance to around 160 $F.g^{-1}$ [23]. CNTs suffer as well from micro pores volume and defects, which are requiring researchers to invent techniques to circumvent these difficulties (such as acid and heat treatments or doping with transition metal oxides)[32].

There are three separate types of CNTs with varying degree of usefulness for supercapacitive applications: Single walled carbon nanotubes (Figure 4) which are made from single wrapped graphene sheets which could be semiconductors with a band gap inversely depending on the diameter of the tube[33].

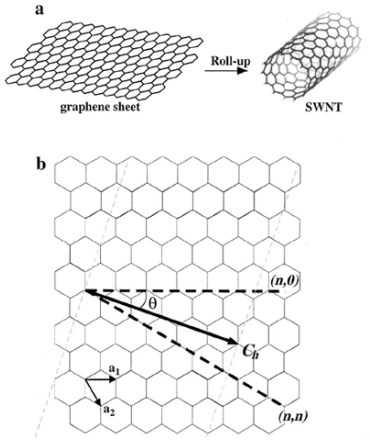

Figure 4- a) Schematic of a single walled Carbon nanotube formed by rolling a single Graphene sheet. b) a 2D Graphene sheet[34].

Multi-walled carbon nanotubes (Figure 5) are several concentrically wrapped sheets of graphene, with an interlayer separation of only a few angstroms. They enjoy a rather modest specific area (400 m^2 per gram) but make up for it in a rather large number of meso pores[35].

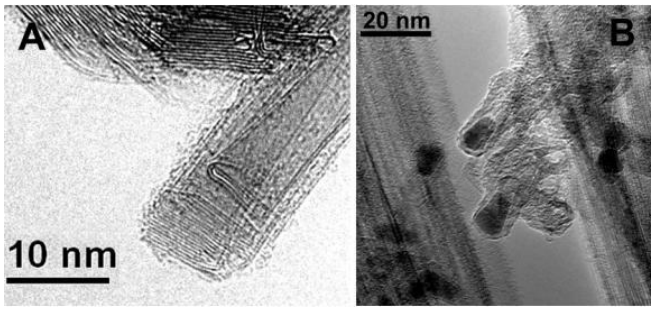

Figure 5 – Transmission Electron Micrograph a mutiwalled CNT[36].

Truncated conical CNTs (Figure 6) are especially attractive as they offer a hollowed tubular morphology, exposes the electrolyte to inner and outer edges of the conical structure[37] whilst still maintaining a long tubular morphology of a nano-fiber. The edges of these conical structures are highly reactive and exhibit high crystallinity[38, 39] good conductivity and promising specific capacitance. However, like most carbonaceous material, the differential capacitance at the edge planes leads to formation of amorphous carbon on the edges and therefore greatly degrades the electrochemical effectiveness of CSCNTs[40].

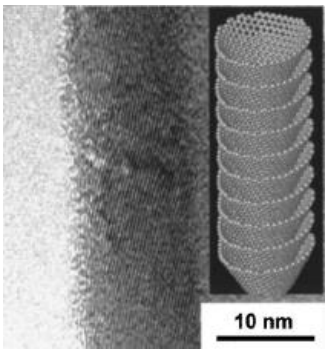

Figure 6- Stack cone carbon nano-fiber showing the average width of the cone[38].

Graphene - based material hold high promise for use as electrodes for supercapacitors due to their unique two dimensional structures[41], excellent conductivity[42], and stability[43], coupled with an extremely high theoretical surface area (2600 m^2/g)[44]. Graphitic sheets can be easily obtained by thermal shock treatment of graphite flakes which preserve their electrical conductivity without limiting their surface area[45]. It could be kept suspended in a solution or given in a paper shape, or incorporated into polymers. In short it is really a dream material. Their surface area is entirely accessible to most electrolytes used in supercapacitors, with a specific capacitance ranging between 95 Fg^{-1} to 160 $F.g^{-1}$ depending on the electrolyte[42]. Extensive work has been dedicated to the study of Graphene based material as possible electrodes for batteries and supercapacitors[18, 42, 44, 46-51]. Graphene being a flexible single sheet of graphite (seem Figure 7 below) was under heavy investigation by various researchers[12], though further activation of the graphitic sheet is needed to increase the number of micro and meso-pores on the surface.

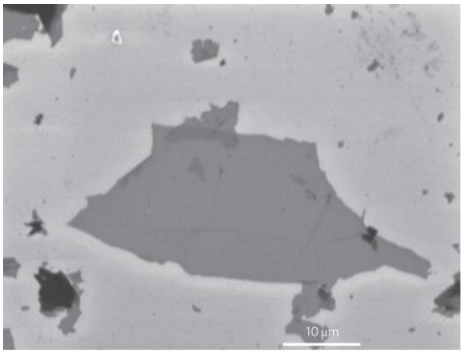

Figure 7- SEM image of a single sheet of Graphene prepared from Hydrazine dispersion[52].

Its excellent conductivity and ease of fabrication, makes graphene attractive as high surface area electrodes for supercapacitors for both academic research and industrial commercialization.

2.2 Pseudocapacitors.

Pseudocapacitors are developed to increase energy density of the previously mentioned double layer capacitors. In this technology the charge storage is based on both the adsorption of ion at the electrode/electrolyte interface as well as the faradic reaction of a redox couple system deposited on the electrode surface. Schematic of pseudocapacitor is shown in Figure 8 below:

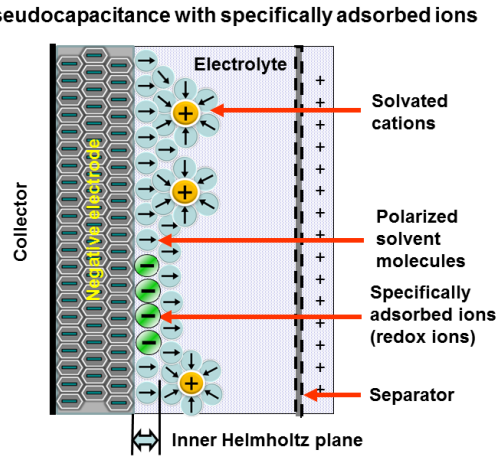

Figure 8-A basic schematic of a Pseudocapacitor showing the adsorption of ions at the electrode/electrolyte interface[53].

The pseudocapacitor benefits from combined faradaic and non-faradaic charge accumulations. It is an energy storage device that works on electron transfer between electrodes through redox reaction and charge storage due the double layer effect. Conway affirms that the charge storage mechanism for pseudocapacitors is similar to batteries' operations than the traditional capacitors[16]. The capacitance obtained from pseudocapacitors could be 10 times larger than EDLCs, however this capacitive behavior is strongly voltage dependent, and its power limited by kinetic factors [54]. Two types of energy storage are possible for a pseudocapacitor: a) The Oxidation/Reduction of transition metal oxides. b) Redox processes of two dimensional material. The difference arises due to thermodynamics reasons such as valency dependent electrosorption of species at the electrode surfaces, where the potential is dependent

on the logarithmic ratios of oxidants and reducers in redox reactions. Conway has also shown that to some extent, the double layer effect at the surface, would still occur even in an entirely pseudocapacitive behavior[55].

Since it was shown that the electrochemical performance of carbonaceous material may deteriorate under the effect of oxidation, which leads to an increase in internal resistance, the interest in these pseudocapacitive devices rose sharply[56]. Transition metal oxides are material sought for pseudocapacitors as they exhibit high specific capacitance and low resistance, and they provide specific energy values higher than carbon. While ruthenium oxides with excellent theoretical capacitance (700 $F.g^{-1}$) were chiefly researched during the infancy of the technology, their commercialization was limited by their cost[57]. On the other hand, manganese dioxide is a cheap, abundant, environmentally benign, and can be easily deposited on a carbonaceous material. The deposition of the manganese is also desirable since hydrating it into an amorphous state greatly reduces its conductivity[58].

It was reported that graphene oxide – MnO_2 nano-composites exhibited a specific capacitance of 210 $F.g^{-1}$ [59]. This could be explained by the pseudocapacitive behavior of MnO_2 adjunct to EDLC phenomena exhibited by graphene oxide. MnO2 enjoys a large specific energy, is environmentally benign and unlike other transition metal oxides considered for capacitor work, MnO_2 is rather inexpensive[60].

Polymers are rendered conductive through a conjugated bond system along the polymer's backbone, which makes them suitable as material for Pseudocapacitor electrodes. When compared with carbon based electrodes, polymers exhibit a lower equivalent series resistance (ESR) and are relatively cheaper[61]. The energy storage in polymers is not electrostatic but results from the insertion and deinsertion of counter ions from the electrolyte[15]. N-doped polymers on one electrode and p-doped ones on the other seem to be the most promising system in terms of specific power. However, n-doped polymers are rare and expensive, and the mechanical stress on the electrodes during charge and discharge greatly reduces the cyclability of the cell[14]. Thiophene-based polymer materials, such as poly(dithien-thiophene) (pDTT1) and poly(3-p-fluorophenylthiophene) (pFPT), are commonly used p-doped polymers, which provide a noticeable improvement to the cell's working potential. Arbizzani[15] showed that the capacitance obtained from n-doped polymers is inferior to those possible from p-doped polymers, however the design of the cell (combining p-doped electrode with an n-doped one) seem to yield a greatly improved result for both capacitance and impedance.

While conductive polymers hold great promise for supercapacitor electrodes, they are not free of drawbacks: As polymers undergo redox reactions to store charge in the bulk of the material, the charge/discharge rate of the cells slows down considerably as compared with a standard EDLC, due to the slow rate of ionic diffusion within the bulk of the electrode. This in turn translates into a reduced power capability: On average, a conductive polymer based supercapacitor (polyaniline for example) can

attain only 2 Kw/Kg, which is a great reduction from a carbon-carbon capacitor which boasts about 4 to 5 Kw/Kg. It is worth noting that is drawback in specific power is balanced by an impressive improvement to energy density (about 10 wh/Kg) when compared with average energy density of an ELDC (3 – 5 wh/Kg)[62].

2.3 – Hybrid Supercapacitors

Since EDLCs have in general lower energy densities than batteries, there is growing need for devices that possess hybrid characteristic of batteries and EDLC. To achieve the goal of a high energy density capacitor, research has been focused on devices that use both faradaic and non-faradaic processes to store charges, which allow them to achieve higher power densities than the carbon-carbon capacitor without being hindered by the low cycle life of pseudocapacitors. Hybrids (Figure 10) also circumvent the problem of gas evolution problem which limits the operating voltage window in the EDLC. While this type of capacitor is relatively new, its theoretical characteristics places it high on the list of desirable energy storage device (see figure 9).

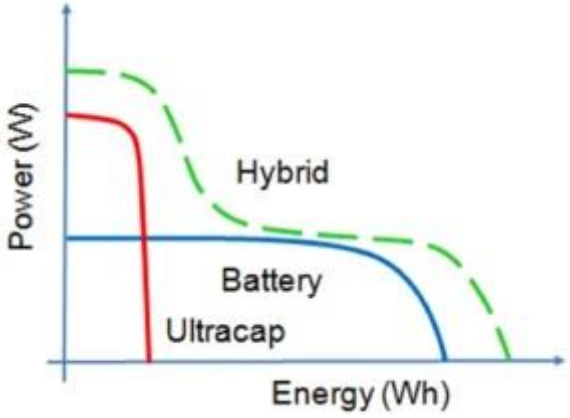

Figure 9- A ragone plot of specific power vs specific energy, showing the highly desirable range for Hybrid capacitors[63].

Asymmetric supercapacitors are hybrids that couple a carbonaceous electrode with a pseudo-capacitive electrode which acts as positive electrode such a NiOOH or $Li_4Ti_5O_{12}$. It is worth noting that while this design delivers a better energy density and cyclability than polymer pseudocapacitors , it still lags behind EDLCs in stability and cycle life[14].

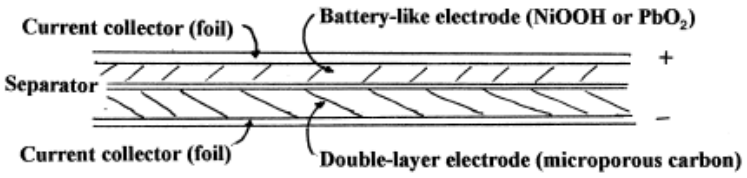

Figure 10- A basic schematic of a Hybrid Supercapacitor: Carbonaceous material on the cathode storing charge electrostatically, and faradic charge storage on the anodic side[64].

Battery-like hybrid supercapacitors are also undergoing active research in recent years. As their name suggests, they couple dissimilar electrodes in hopes of gaining the high energy density from the battery electrode and higher power density from the carbonaceous one. Data about these devices is still lacking as research is progressing slower on this front than the other type of capacitors. The most widely researched hybrid is the lithium ion capacitor with electrodes made of activated carbons or graphite is coupled with high rate electrodes such as $Li_4Ti_5O_{12}$. It is the marriage of a lithium ion battery on the negative side and an EDLC on the positive electrode. The reactions taking place in such a system are unique: Li+ cations are intercalated and de-intercalated on

the anode with an SOC less than 50% whilst the usual adsorption and dis-adsorption of anions happen at the positive electrode, allowing for both a higher voltage and higher specific energy[65]. This system is not without draw backs: The high voltage window causes some metal deposition which in turn increases the impedance at the electrode/electrolyte interface with each cycle. The future of hybrid capacitors would require addressing these interfacial issues. One method under investigation employs $Li_4Ti_5O_{12}$, which operates in a voltage window out of the range where electrolyte decomposition may occur. As a nano sized redox material for hybrids, $Li_4Ti_5O_{12}$ promises a theoretical capacity four times larger than those provided by EDLC, and shows very little sign of degradation or gas evolution. Work is being done to couple $Li_4Ti_5O_{12}$ and carbon nano fibers, which is exhibiting high power and high energy densities. Results on this front are yet too preliminary.

Finally, composite hybrids are certainly the most popular, and stable of hybrid supercapacitors: Two identical electrodes made by integrating a transition metal oxide (TMO) into carbonaceous material. These capacitors manage to circumvent most deficiencies in pseudocapacitors, and enjoy the long cycle life associated with EDLCs (10^6 cycles). Several systems have been tried and reported such as carbon nanotubes and polypyrrole, graphene and MnO_2, graphene and Mn_3O_4 and so on. Recently one such system has been gaining in popularity which is a composite of NI (OH) 2/multiwalled carbon nanotube with adequate capacitance and superb cyclability. In such system, the activated carbon (AC) electrode stores charge through surface localized non faradaic ion

adsorption/desorption, while the other electrode utilizes the reversible redox reaction of a transition metal oxide or a lithium intercalated compound. The immediate benefits of such a system result from the high working voltage of the battery-like electrode which of course leads to an increase in the energy density of the overall cell[66].

2.4 – Electrolytes for supercapacitors

Currently electrolytes used in supercapacitors are either aqueous, organics, or ionic liquids (liquid salts). Typically these salts are dissolved in one or more solvents, before being suited to the type of electrodes employed in the design of the cell. Several criteria are demanded of electrolytes for supercapacitors: Electrochemical stability over a wide voltage window, and a good degree of dissociation of the selected salt into free ions, which would lead to good ionic conductivity. The latter is crucial in maximizing specific power of the cell which is given by the following:

$$\boldsymbol{P} = \frac{\boldsymbol{V^2}}{\boldsymbol{4.m.ESR}} \qquad \textbf{(4)}$$

Where P is the power in w/Kg V is the maximum stability voltage of the supercapacitor, m is the weight of the supercapacitor, and the equivalent series resistance (ESR) is the sum of all resistances of the cell from ionic resistance in the electrolyte, to interface resistance between the electrodes and the electrolyte as well as the electronic resistance of the electrodes themselves. Solvents used must also enjoy an electrochemically stable cycle life and show good ability to solvate the salt ions[67].

Generally, alkali and acidic electrolytes such as potassium hydroxide (KOH) and sulfuric acid (H_2SO_4) enjoy good conductivity but are hindered by the narrow voltage window (around 1.23v) due to the dissociation of water molecules. Some work has been done to widen this operating window through the optimization of the carbon material used as electrodes[68, 69]; however this hindrance is pushing research towards organic electrolytes which enjoy a wider operating window, despite the fact that neutral aqueous electrolytes showed promise in extending the voltage of window of supercapacitor cells.

Ionic liquids are molten salts that have been gaining momentum as candidates for supercapacitor electrolyte. They consist of ions and their combinations and are solvent free. For these salts to be useful in supercapacitor application, they must have a low melting point so that they can remain in a liquid phase at room temperature. In the 1990s new ionic liquids were described, based on 1-ethyl-3-methylimidazolium cation and tetrafluoroborate anion, resistant to moisture traces, and hold great promise as electrolyte for supercapacitors. Other examples are tetralkylammonium, or pyridinium, but the use of those salts have been hindered by their low conductivity. Ionic liquids enjoy a rather wide operating voltage window (between 3 and 4 volts) which makes them ideal for improving the energy density of the supercapacitor, however further research is needed on ionic liquid to optimize their use[70].

Commercial supercapacitors often use organic electrolytes. These are salts dissolved in an organic solvent which in turn provides a wider operating voltage (2.5 to 2.7v) which provides higher specific energy for the supercapacitor cell. The stability of this operating voltage is strongly dependent on the nature of the electrolyte and the residual water content in the electrolyte. Therefore in industry, several purification methods as well as dry electrode coating processes are employed to ensure the stability of this electrochemical window. Propylene carbonate (PC) and acetonitrile (AN) are the most commonly used solvents in supercapacitors, and both present advantages and come with their own sets of drawbacks as well: The high viscosity of Propylene carbonate makes the supercapacitor cell a lot more sensitive to temperature variation, whilst acetonitrile containing salt may precipitate during cell ageing, due to reaction with electrodes on long exposure[71, 72].

Chapter 3

Fabrication and Characterization Methods of Supercapacitor Electrodes

Graphene is a unique two dimensional material with excellent qualities in the several physical domains such as optical electrical and mechanical. Its use in electronics and sensors and various other applications was also driven by its low cost, and relatively effortless method of synthesis. Among the various methods of synthesis, Hummers' method proved to be the most effective in terms of safety and satisfactory outcome [73], though other methods have been used to produce exfoliated graphite, such as microwave assisted exfoliation[74], chemical reduction of graphene oxide or simple micro-mechanical exfoliation[75]. The exfoliation process may expand graphite to near a hundred times along its C-axis. The expanded graphite flakes are flexible, conductive, heat resistant, and enjoy a large surface area, and extreme sorption capacity[76, 77]. Care must be taken when rapidly expanding graphite as oxygen group tend to form chemical bonds at the edge and in between the layers, in particular, at the defect sites, and further reduction of the formed expanded graphite would be required. In our study, we subject graphite flakes (obtained from Sigma-Aldrich) which were presoaked in sulfuric acid, to a thermal shock, by introducing them to a preheated box oven set at 1100^{o} C. The flakes expanded along their c-axis as expected and had a fluffy serpentine shape. Based on previous work done on this exfoliation process, we expected our sample to have larger surface area, with pores varying in diameter (190 to 320 μm)[78].

3.1 Fabrication of Supercapacitor Electrode Materials

a) Exfoliated graphite:

0.1 g of as prepared Exfoliated Graphite (EG) was soaked in 30 ml of N-Methyl-2-Pyrrolidone (NMP) solvent (purchased from Alpha Aesar) and placed in a sonication bath for 24 hours: The serpentine EG lost its fluffiness at first and formed black agglomerations at the bottom of the beaker, then dispersed to form a homogenous black solution of graphite/NMP. While undergoing vigorous stirring with a magnetic bar, 100 ml of 1 molar potassium hydroxide (KOH) (obtained from Alfa Aesar) solution was added drops wise to our EG/NMP solution. The solution was allowed to stir for half an hour before being refluxed at 100^{o}C for 48 hours. The sample was dried, and the agglomerate of EG and KOH was annealed under Argon/Hydrogen environment for two hours at 600^{o}C, in order to activate the carbon by creating pores on the surface. This activated carbon mixture was then washed thoroughly to bring the PH down to neutral and filtered. The resulting activated carbon was dried on a hotplate in air at 70 ^{o}C then collected. By adding 20 ml of solvent (NMP), a slurry of ink-like consistency was formed to coat our electrodes: Pre-cleaned nickel foam substrates were then dipped in the EG-NMP solution for a few minutes to allow the material to enter the pores of the foam. The electrodes were dried using a heat-gun to evaporate the NMP. As formed electrodes were then weighed to determine the amount of EG loaded in each, and then used in a three electrode system to determine their electrochemical properties.

b) Exfoliated graphite/MnO2 nano-composite:

0.13 g of Potassium Permanganate ($KMnO_4$) powder (Purchased from Alfa Aesar) was added to a beaker containing 20 ml of deionized water. After stirring for about an hour at room temperature to ensure proper dissolution, 0.1 grams of the activated EG were slowly added to the beaker and allowed to stir until proper wetting of the graphite was achieved. The beaker was then placed in a sonication bath for 48 hours at room temperature. The shear forces that give birth to voids in the liquid due to fluctuations in the pressure, serve in further exfoliating the EG and allow the good soaking of carbon in the potassium permanganate solution. While undergoing vigorous stirring in an ice bath, hydrogen peroxide (H_2O_2) (Sigma Aldrich) was introduced drop wise into the solution. The color changed from violet to deep brown and then to dark black signifying an oxidation of the previously reduced potassium permanganate to final product, the nano-sized MnO_2. The sample was allowed to stir for 30 minutes to return to room temperature, then washed with plenty of distilled water and filtered. After drying at 70 ^oC overnight, the formed filtrate was characterized via X-ray Diffraction and SEM. A paste was prepared by ball milling the filtrate in presence of NMP for 15 minutes. Electrodes were prepared for electrochemical testing as described above.

c) Exfoliated graphite/MnO2/Carbon nano-fiber composite:

The desire to combine the double layered effect of the EG-CNF mixture with the pseudo-capacitance of MnO2 drove to test the combined effect of the mixture:

Equal amounts of activated EG and CNF were dispersed in NMP under sonication for two days. The liquid was homogenous and well dispersed. We added an equal part of KMnO4 dissolved in deionized water to the beaker whilst undergoing rigorous stirring. After ten minutes of mixing, the $KMnO_4$ start to reduce in presence of NMP to form Mn_3O_4 with its distinctive brown color. We then drop wise introduce hydrogen peroxide to the mixture to further reduce the previously formed manganese (II, III) oxide into MnO_2 phases. The formed black mixture was washed with copious amounts of deionized water and dried overnight. The dried filtrate was characterized via x-ray diffraction and scanning electron microscopy. Slurry was then made by ball-milling the filtrate in presence of NMP. Electrodes were made for electrochemical testing.

Electrodes were made by coating pieces of Nickel foam with the respective slurries, Nickel foam was chosen because of its good conductivity, large number of pores and high surface area. Pre-cleaned pieces of nickel foam were weighed before being dipped in the various solutions prepared above. After drying, the now coated nickel pieces were weighed again to determine the loaded mass of active material.

3.2 Characterization of Supercapacitor Electrode Materials

3.2-1 X-ray diffraction

X-ray diffraction measurements were conducted using Rigaku MiniFlex diffractometer (Figure 10) (λ = 1.54 Å) with Cu-Kα radiation operated at 40 kV and 15 mA.

Figure 11: Rigaku XRD

When an x-ray beam diffracts off a crystal as shown in Figure 12, angles and intensities of the diffracted beams are commonly used to identify atomic and molecular structure of the crystal. This is possible because the wavelength of x-ray is comparable to the interatomic spacing of materials. Following Bragg's law, the position and the intensity of the diffracted x-ray beam can inform us on the size and geometry of the unit cell.

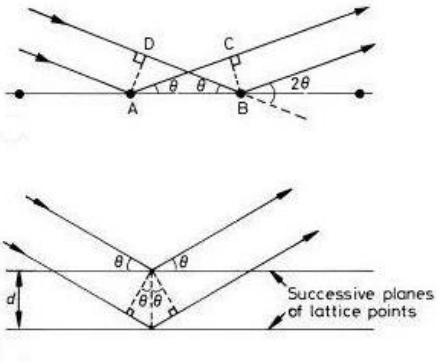

Figure 12- Classical schematic of reflection of a beam of light from a reflexive surface[79].

An X-ray crystallographer would employ Miller indices to label different reflection off the planes forming the crystal lattice. The inter layer spacing of the reflected beam correspond to the angle of diffraction according to the Bragg's law:

$$2dsin\theta = n\lambda \qquad (5)$$

Where θ is the diffraction angle, λ is the wavelength of the x-rays and *n* is the order of diffraction[79].

The crystallite size D may also be determined by using the Scherrer's equation:

$$D\beta cos(\theta) = K\lambda \qquad (6)$$

Where, β is the full-width-at-half-maximum (FWHM) of the XRD peak and K is the dimensionless Scherrer constant, which is heavily dependent on the size and shape of the crystal, but normally taken to be (0.9). Typically a θ - 2θ scan is performed in such a way that an incident wave is reflected at an angle 2θ after being incident at an angle θ.

3.2.2-Scanning Electron Microscopy

Scanning Electron Microscopy (SEM) images were obtained using JSM-6510-LV-LGS SEM operating at 25~30 KV.

A focused electron beam is used during Scanning Electron Microscopy to scan a sample specimen. This irradiation of the sample's surface by this focused electron beam

helps in creating images helpful in studying the morphology of the sample. Quality of the images produced is greatly dependent on the conductivity of the material which is why a gold coating is applied to the surface of the sample prior to irradiation. Some of the probing focused electrons will penetrate the sample to a certain depth resulting in a collision with a surface atom and four characteristic scattered beams are produced and are shown in Figure 15:

Secondary electrons: Used to deduce high resolution topographic information about the surface scanned. These secondary electrons have low energy (a few eV) they result from the interaction of the primary beam with the surface of the sample. Charging effect which is displayed by distorted white flashes in the image produced is normally due to the charging of the non-conducting material in the sample.

Backscattered electrons: Primary beam electrons scatter off the surface and are re-emitted with little loss in energy. The main function of these backscattered electrons is to modulate the contrast of the images formed. Detection happens along large area semi conducting diodes.

X-rays are also generated during SEM which is characteristic of the sample being studied. These photons are generated due to electronic transition created by the vacancies in atoms being irradiated by the electrons beam. The rays are used to characterize of the specimen being studied.

Scanning Electron Microscopes have been produced commercially since 1965 and have evolved much though the years, increasing magnification and reducing energy requirements. Figure 13 below shows a very basic schematic of a scanning electron microscope. Its use has spread into every branch of science such as polymer studies as well as ceramics and metals. SEM imaging of semiconductors is wide spread, and considered now to be standard characterization tool for most nanomaterial.

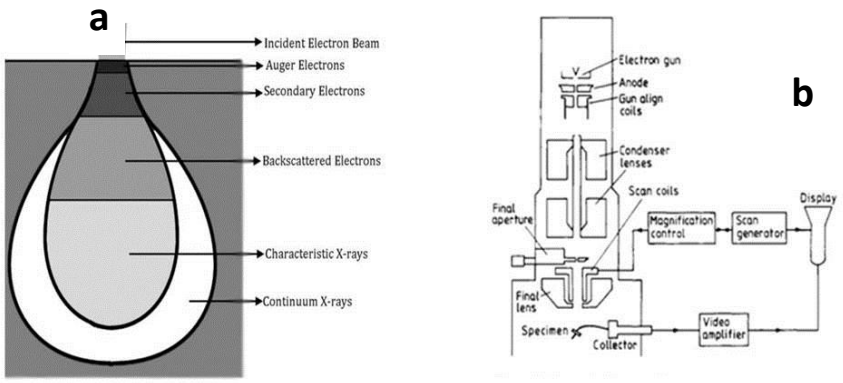

Figure 13- a) A spectrum of backscattered electron beams generated during SEM[79]. b) Schematic of a Scanning Electron Microscope[80].

For supercapacitors, SEM provides information about surface morphology and particle size of electrode material as well as separator membrane porosity. Usually images are obtained before and after chemical activation of material to study the effect

on the phase and morphology of the sample. More importantly, during the study of Pseudocapacitors, SEM would be used to study the transition metal oxide particles' location in correspondence to the carbonaceous material.

3.3-Electrochemical Measurements

A Gamry potentiostat operating with a Gamry 1800 software was used to perform electrochemical measurements on our prepared electrodes in a three electrode cell (see Figure 14 below), using an aqueous electrolyte of a 1 molar sodium sulfate Na_2SO_4. The electrolyte contains Na^+ and SO_4^{2-} ions, that may adsorbed on electrode surface and also provide ionic conductivity within the separator medium.

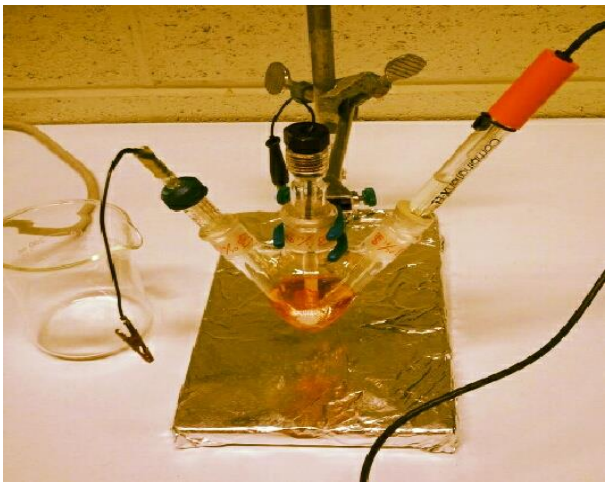

Figure 14- Three electrodes set up for testing supercapacitor material: A platinum mesh electrode as a counter electrode a working electrode in the middle to hold the sample and a Calomel reference electrode on the right.

The MnO_2 may also go under reduction process to form MnOOH and $Mn(OH)_2$ specious on the surface of the MnO_2 particels.

$$MnO_2 + H^+ + e^- \rightarrow MnOOH \text{ and } MnOOH + H^+ + e^- \rightarrow Mn(OH)_2$$

the intercalation of the H^+ protons or the Na+ cations in the bulk of the material upon reduction[81].

The three electrodes cell setup was chosen because it allows for electrochemical tests to be conducted rapidly while providing useful information about reaction kinetics, and the energetic of the various redox couples on the electrode surface.

3.3.1 Impedance Spectroscopy

In later half of the nineteenth century O. Heaviside's mathematical transformations laid the ground for electrical engineering as we know it today, and defined impedance as

$$\boldsymbol{Z(S) = \frac{V(S)}{I(S)}} \qquad \textbf{(7)}$$

where S is the Laplace frequency[82].

Impedance spectroscopy is a widely used technique to investigate electrochemical systems. The advantage of EIS is that it is generally non-destructive to the investigated system. Heaviside realized that his transformations into the Laplace space are only valid for a non-perturbed system. This of course comes from the desire to

describe the analyzed system with linear differential equations. This enables the possibility for further electrochemical measurements and post-mortem investigations. EIS is the most common method for measuring the equivalent series resistance (ESR) of ECs. It also allows creating models to describe underlying reaction mechanisms. With these models capacitor non-idealities also can be investigated:

Generally, a sinusoidal AC excitation signal is applied to the investigated system during an EIS experiment and the AC response is measured. The frequency of the input signal is varied during the measurement. Finally, the impedance *Z* of the system is calculated.

The modern form of the impedance function:

$$\boldsymbol{Z(\omega) = \frac{\sigma}{\omega^{\frac{1}{2}}} - \frac{j\sigma}{\omega^{\frac{1}{2}}}} \qquad \textbf{(8)}$$

was introduced by Emil Warburg in a now famous paper published in 1889. Where Z (ω) is the Warburg impedance, ω is the radial frequency and σ is the Warburg coefficient defined as

$$\boldsymbol{\sigma = (RT)/(n^2F^2A\sqrt{2})\left(\frac{1}{C^{*o}\sqrt{D_o}} + \frac{1}{C^{*R}\sqrt{D_R}}\right)} \qquad \textbf{(9)}$$

in which D_0 is the diffusion coefficient of the oxidant, D_R is the diffusion coefficient of the reductant, A is the surface area of the electrode, F is the Faraday constant,n the

number of electrons involved and C^{*o} is the bulk concentration of the oxidant, C^{*R} is the concentration of the reductant.

When an electron is transferred through the diffusion layer of an electrified surface, non-faradaic components to the current generated result from charging of the double layer capacitor (C_{dl}). This flow of current through the faradaic reaction is modeled by the following:

$$\textit{Oxidant} + ne^- \rightarrow \textit{Reductant} \qquad (10)$$

An electrochemical technique capable of providing equivalent circuit components of an electrochemical cell. For the case of a supercapacitor, a typical impedance spectroscopy can be modeled by the equivalent circuit (Fig. 15)

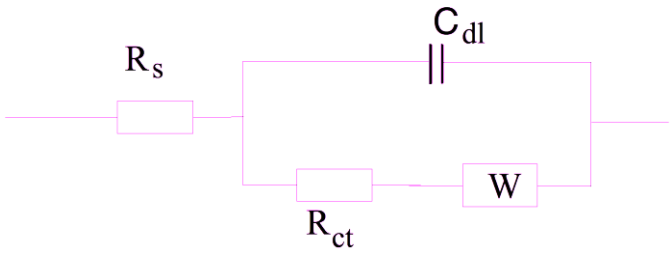

Figure 15-Equivalent Circuit Diagram of an electrochemical capacitor[83, 84].

where n is the number of electrons that need to overcome the polarization resistance (R_{ct}) as well as the electrolyte resistance (R_s). The semi-circle resulting from a typical EIS has a radius of $R_{ct}/2$ with a high frequency intercept of Rs and a low frequency intercept of $R_s + R_{ct}$. (Fig. 16) Here R_s is the electrolyte resistance, R_{ct} is the charge transfer resistance, and C_{dl} is the double layer capacitor. The maximum on the semi circle

represent the time constant (RC) for the system. The Nyquist plot of impedance provides information about the equivalent resistance of a supercapacitor as well as a good model for its ionic transfer. A sample Nyquist plot is shown in Figure 16 below:

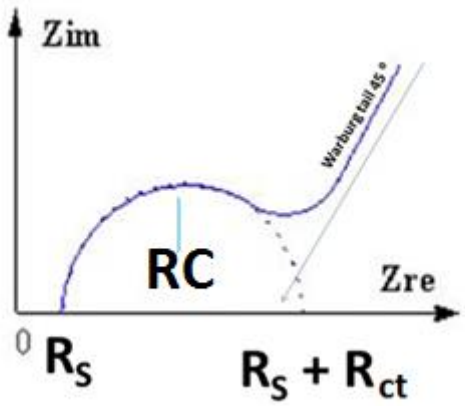

Figure 16-Nyquist plot of the galvanostatic Impedance of a few electrodes[85].

The Warburg "tail" is a good indicator of the diffusion of ionic species, for an ideal EDLC behavior, the tail is nearly vertical, due to the fast response and a good stacking of the ions on the carbon pores in the Helmholtz layer and a relatively smaller diffusion layer. Figure 16 above shows a Nyquist tail sloped at 45^o which is traditionally linked with battery faradaic behavior, where faradaic reactions are used to transfer charge into the electrode.

3.3.2 Cyclic Voltammetry

The Gibbs and Nernst equations are used to predict the potential for an electrochemical cell.

$$\Delta G = -nFE_{cell} \qquad (11)$$

Where ΔG is the Gibbs free energy of the chemical reaction, n is number electron exchange in the reaction, and F is the Faraday's constant, and E_{cell} is the theoretical cell potential. The cell potential is also depends on the concentration of reactants and products according to the Nernst equation:

$$E_{cell} = E^{0}_{cell} - \left(\frac{RT}{nF}\right) ln\left(\frac{Cox}{Cred}\right) \qquad (12)$$

However, the practical cell voltage is less than the predicted value by the above equations, due to various voltage losses, including activation, ohmic and concentration over-potentials. Cyclic voltammetry (CV) is one of the most reliable and sensitive methods for studying electrochemical reactions. The CV measures the current response of an electrode as a function of applied voltage. The importance of this technique lies in its ability to provide reaction potential, and adsorption processes at the electrode/electrolyte interface. In cyclic voltammetry, the potential of the working electrode is ramped linearly using a triangular potential scan against a reference

electrode which is maintained at constant potential. Figure 17 shows the triangular voltage sweep versus time commonly used in cyclic voltammetry measurements.

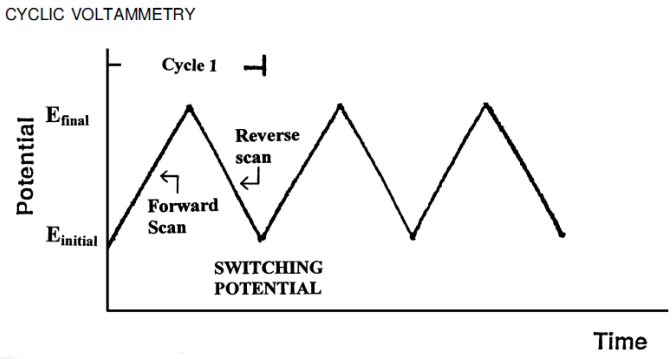

Figure 17: Schematic of triangular voltage scan vs. time used in cyclic voltammetry[86].

The excitation signal above, which is the controlling potential applied between the working electrode and the reference electrode, reaction potential where oxidation-reduction reaction happens in the cell. The upper and lower voltage limits are selected to include the redox reaction potential under study. The sweep rate is given by the slope: $\frac{\Delta V}{\Delta t}$.

The redox reaction at the electrode produces current that will be monitored during the voltage sweep. The cyclic voltammogram typically displays the current on the vertical axis and the potential on the horizontal one. An ideal capacitor with no impedance, would display a rectangular voltammogram, as shown in figure 18.

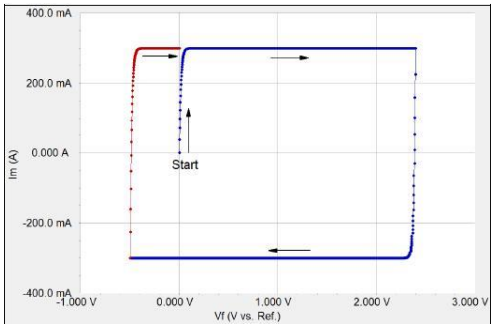

Figure 18- Theoretical CV curve of an ideal 3 Farad EDLC[84].

however there is often presence of redox reactions near the electrode surface which may produce oxidation and reduction peaks [51]. The formation of concentration gradient in the ionic diffuse layer near the electrode also produce changes in the ideal rectangular shape of the voltammograms, as shown in Figure 19.

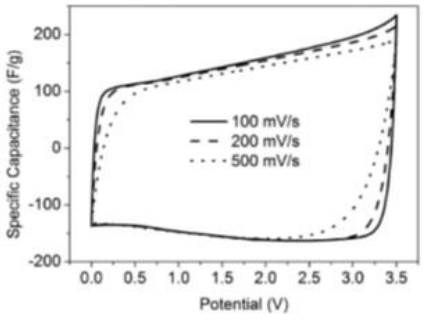

Figure 19-A voltammogram of an activated Graphene electrode where a forward scan was initiated at 0 volts[51].

The anodic current will oxidize the material and the cathodic current corresponds to a reduction process. The peak observed around 3.5v corresponds to oxidation of carbon surface groups and possibly the beginning of electrolyte

decomposition. This process will continue until such time as the anions concentration is diminished enough to cause a dip in the current at which point the scan is reversed.

Charging or discharging the capacitor at higher sweep rates would demonstrate its behavior at higher power demand. A supercapacitor, with good cyclability provides mirror image charge and discharge curves in a CV plot.

Chapter 4

The exfoliated graphite/carbon Nano-fiber/MnO_2 nannocomposite supercapacitor electrode material.

4.1 Structural characterization

4.1.1 X-ray Diffraction Measurements

The XRD patterns of various samples and their components showed great agreement with the reported literature. Figure 20 below presents the diffraction patterns for pristine Graphite. The strong (002) peak around 26.5^o and 75^o which is a characteristic peak of carbon.

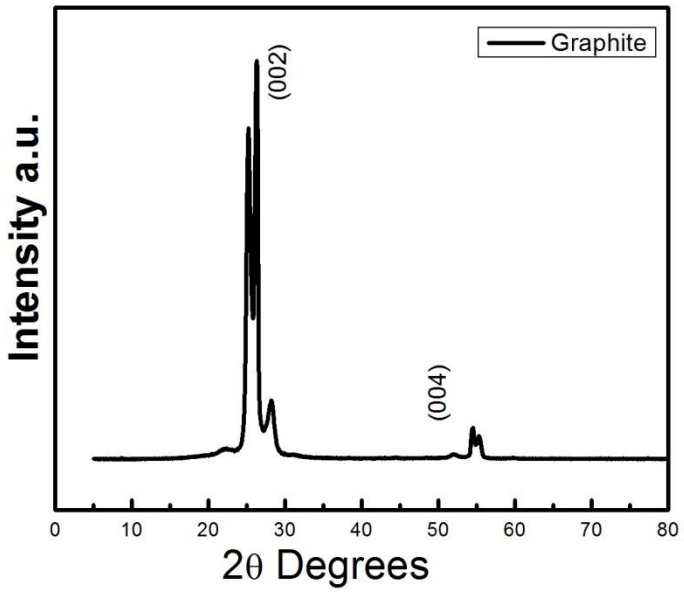

Figure 20- XRD of Graphite soaked in concentrated acid showing characteristic peaks at 26.5, 26.7 and 54.2 degrees, indicating various stages of graphite intercalation with acid.

The inter layer distance between the graphene planes are reported in literature[87] indicated that the interlayer spacing was about 0.314 nm. The diffracted beams at lower 2-θ correspond the expanded interlayer distance of graphene due to intercalation of acid between some of the graphene planes. However, most part of the graphite structure has remained unperturbed with no intercalation. The multiplicity of the XRD peaks around 26.7 have been resulted due to the formation of various stages on acid intercalation, providing different inter-layer graphene distances.

Figure 21 shows the X-ray diffraction pattern of exfoliated Graphite. The persistent presence of the (002) at 26.7° and (004) at 54.2° peaks in the EG sample is an indication that the intercalated acids between the graphene planes are removed due to the heat treatment, and the pure graphitic part contribute mostly to the diffracted

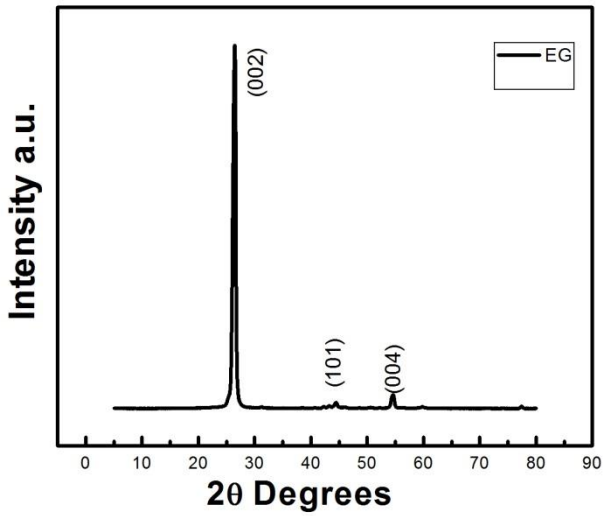

Figure 21- XRD of Exfoliated Graphite. There is not shift in the peaks at 26.5° or at 54.2°.

beam. The interconnected Graphitic sheets still exist. The full width at half maximums (FWHM) at 26.5^{o} increased after thermal shock treatment indicating a reduction in the particle size, and disorder in stacking of graphene sheets. The fact that we observe single (002) peak with no peak between the Graphite and the Exfoliated graphite, despite the reduction in size of the crystallites, which could be an indication of complete removal of the intercalated acids[88].

To contrast, Figure 22 below presents the diffraction pattern of the cone-stack carbon nano fiber.

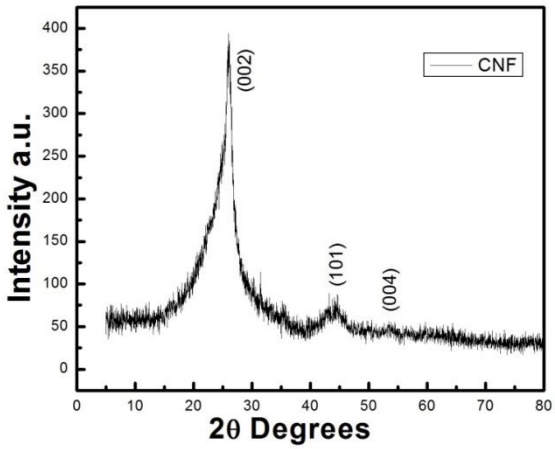

Figure 22- Xrd patterns of CNF, showing the characteristic peaks of Carbon.

The characteristic carbon peaks at 26.2^{o} (002), 44.5^{o}(101) and 53.4^{o}(004) are present in both sample and match precisely with those reported by Fujimoto[88] and Zhou[89]. There is broadening of the (002) peak which may be due to disorder and strain

on the lattice site, and a reduced size of the particles. The Scherrer equation is used for particle size reduction:

$$\boldsymbol{D = \frac{K\lambda}{\beta sin\theta}} \qquad \textbf{(12)}$$

D being the means size of the ordered crystalline domain, β is the broadening at half the width intensity (FWHM) and θ the Bragg angle, can be used to determine the particle size and in the case of CNF we obtain 2.3 nm at (002).

These Carbon peaks were also observed in the other sample containing Manganese Dioxide (MnO_2) as shown in Figure 23 below. We notice that our synthesis method have reduced the $KMnO_4$ into two different phases of MnO_2: α-MnO_2 crystals with peaks at: 28.9°(311), 36.6°(400) and at 42°(301) and Ramsdellite MnO_2 with peaks at: 43.8°(401), 65.1°(020) and 69.5°(303).

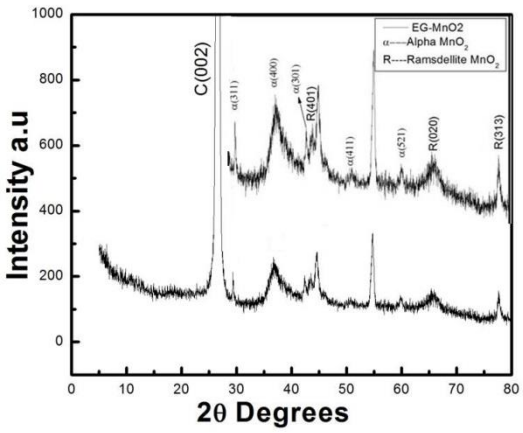

Figure 23- A scaled view of the X-ray diffraction pattern of EG-Manganese Oxide composites. The peak positions corresponding to MnO_2 are in agreement with those reported in literature. The intense graphite (002) line is shown around 26.7 °.

The same varying phases of MnO_2 could also be observed in the EG-CNF-MnO2 composite as shown in Figure 24 below.

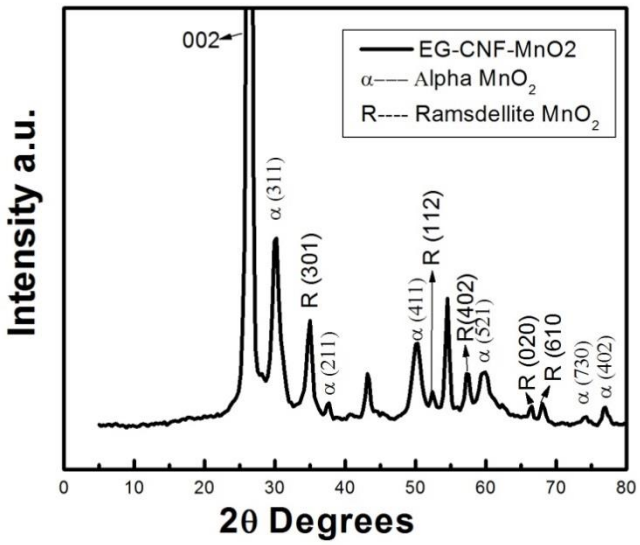

Figure 24-XRD patterns of EG-CNF-MnO_2 composite.

The Carbon peaks are present and so are the (311), (301) and (411) peaks corresponding to Alpha MnO_2 in addition to those peaks characteristic of Ramsdellite MnO_2 such as (401), (020) and (313). The main observable difference that the addition of CNF to the Exfoliated Graphite sample containing MnO_2 is a sharpening of the peaks which may indicate lessening of the strain on the crystalline structure and a further increase in the particle size.

4.1.2 Scanning Electron Microscopy (SEM)

SEM images of the various samples are presented below:

The Graphitic flakes of different sizes extending over 10 microns in x and y axis, and with many layers of stacked graphene sheets along their C axis. It is along this axis that we see the expansion upon exfoliation through thermal shock, as shown in Figure 25. The expansion of the graphite appears to have reduced the number of the stacked graphene layers and increased their interlayer spacing. The size of the graphite sheets as apparent from the images seems to be on the order of 300 nanometer.

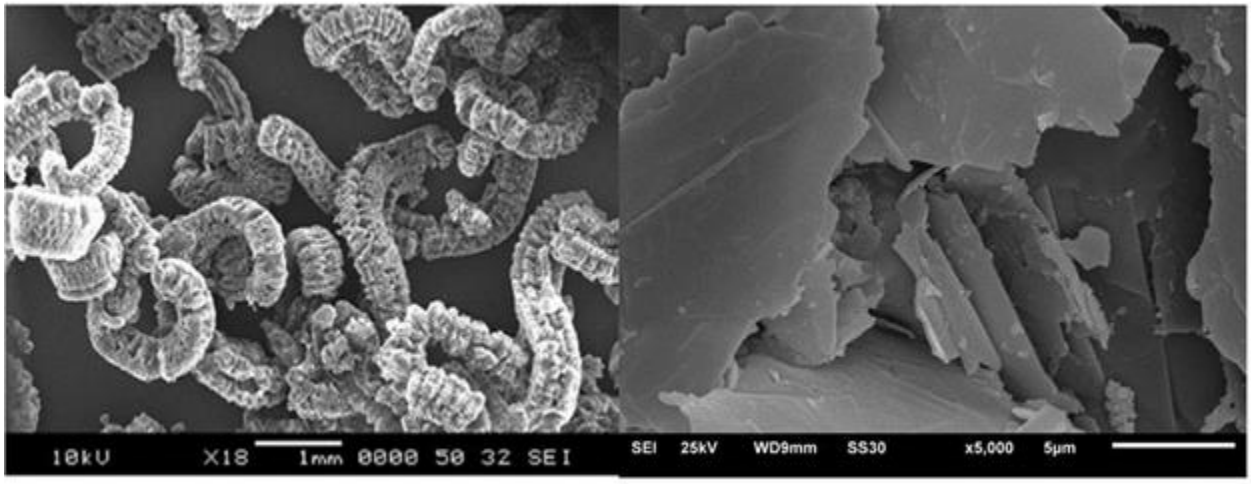

a b

Figure 25- a) Worm-Like Exfoliated Graphite. b) SEM image of Exfoliated Graphite.

In addition to further increasing the surface area of the electrode, we have added carbon fiber to the exfoliated graphite. Figure 28 shows the morphology and aspect ratio of the carbon Nano-Fiber (26 a) and the composite of Carbon Nano-Fiber and the expanded graphite (26 b), as a suitable substrate for the Pseudocapacitor. The

dispersion of the carbon fibers on the graphite flakes as well as in the pores created during activation might be an indication of good capacitive behavior though the double layer effect.

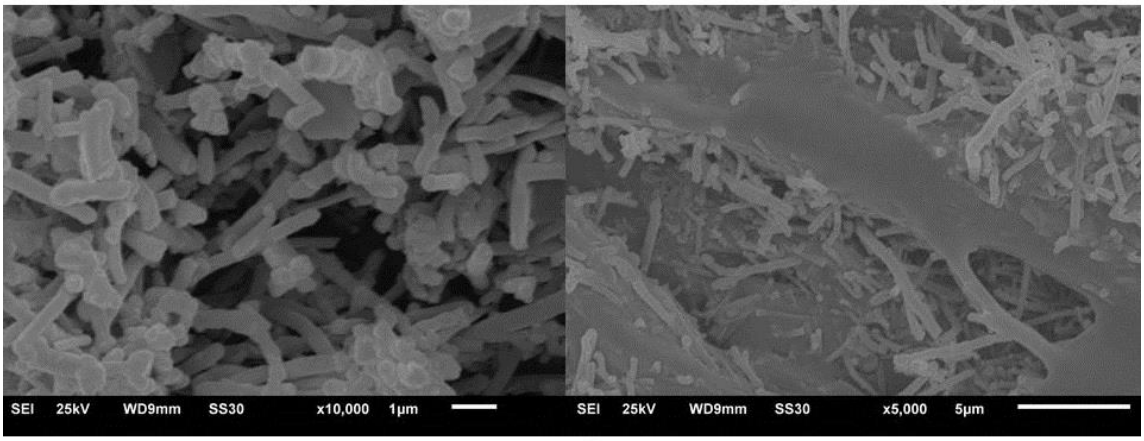

Figure 26- a) SEM image of cone stack Carbon Nano-fiber. b) SEM image of a mixture of Exfoliated Graphite and Cone Stack Carbon Nano-fiber.

In order to enhance the overall capacity of our Supercapacitor, we have deposited nano sized Manganese dioxide (MnO_2) on the exfoliated graphite. Figure 27 shows the morphology and uniform distribution of MnO_2 particles on exfoliated graphite. The Manganese oxide particle sizes are between 60 and 100 nm. This disparity may be attributed to the varying phases of MnO_2 formed during synthesis.

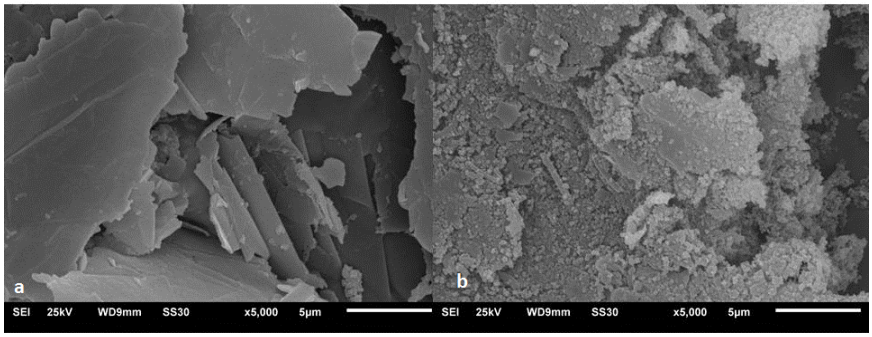

Figure 27- a) SEM image of exfoliated graphite. b) SEM image of a mixture of exfoliate graphite and manganese dioxide.

In the final stage, we made composite containing Exfoliated Graphite (EG) – Carbon Nano-Fiber (CNF) containing Manganese dioxide (MnO_2) nano particles. Figure 28 a, shows the SEM images of the Exfoliated Graphite (EG) – Carbon Nano-Fiber (CNF) (28 b) and the Exfoliated Graphite – Carbon Nano-Fiber, containing Manganese dioxide (MnO_2).

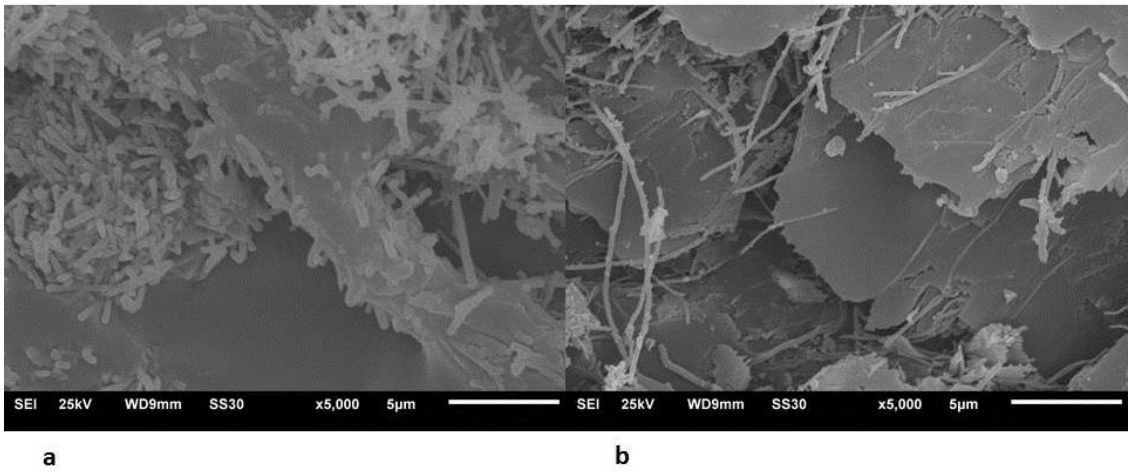

Figure 28- a) SEM image of a mixture of exfoliated graphite, carbon Nano-fiber. b) SEM image of a mixture of exfoliated graphite, carbon nano-fiber and MnO_2.

A uniform dispersion of Carbon Nano-Fiber on Exfoliated Graphite is clearly seen with good connectivity. The Manganese Dioxide (MnO_2) particles with varying sizes are present on the tubular fibers as well as on and between the Graphitic layers. This is a good indication of the sought after uniform dispersion of materials in the composite. The electrochemical performance of the samples discussed above is reported in the following section.

4.2 Electrochemical performance

4.2.1 Electrochemical Impedance Spectroscopy (EIS) measurements

The impedance spectrum of the exfoliated graphite impregnated into the Nickel foam is reported in Figure 29.

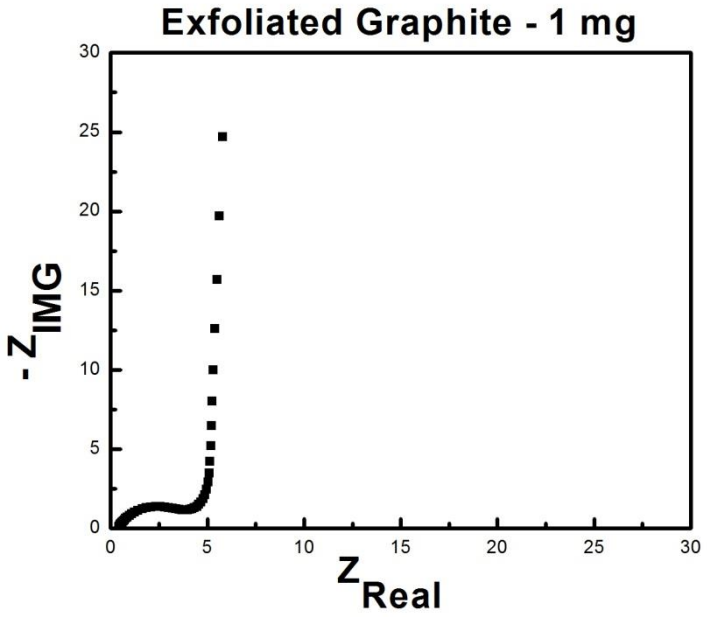

Figure 29-Impedance Spectroscopy measurement of a 1mg electrode of exfoliated graphite (EG).

A very low resistance (<10 Ohms) is observed for the combined electrolyte and the charge transfer resistance (the intercept of the semi-circle with the Z_{real} axis). A sharp rise in $Z_{imaginary}$ due to the Warburg impedance is also observed, which is characteristic of the diffusion of the ions in the diffuse layer next to the electrode. The initial intercept of the impedance plot, representing the electrolyte resistance is less than 1 ohm.

Impedance spectroscopy of the Exfoliated Graphite and Carbon Nano-fiber composite deposited on nickel foam is shown in Figure 30.

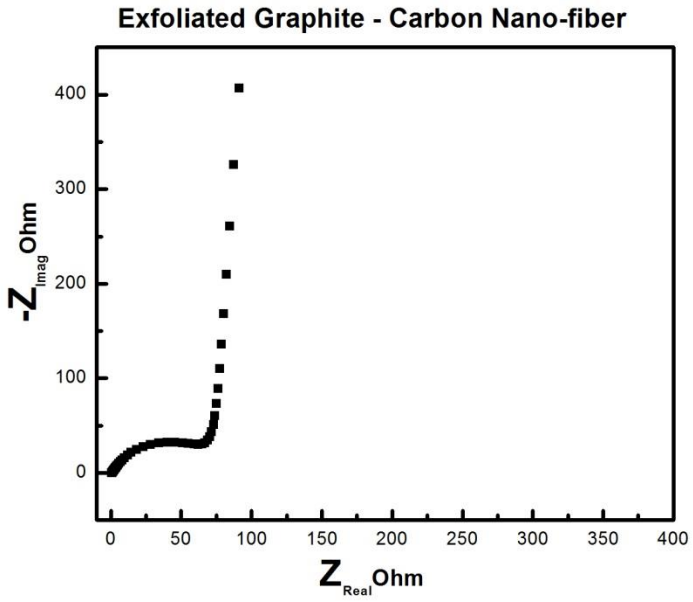

Figure 30- Impedance spectroscopy measurements of a 1 mg electrode of an EG-CNF composite.

As shown by the intercept of the semi-circle with Z_{Real} axis, the charge transfer resistance is much high in the Cone-stack Carbon Nano-fiber sample (around 60 Ώ), however the sharp slop of the "tail" on low frequencies indicate a good double layer effect in the sense that the width of the diffusion layer is small compared to the Helmholtz layer on the electrode/electrolyte interface.

A marked increase in the charge transfer resistance (> 60 Ohms) is observed. This result indicates that carbon Nano-Fiber is less conductive than the graphene sheets. However, the interlacing of carbon Nano-Fiber between the layers of the Exfoliated Graphite provides a more open space with exposed surfaces.

Impedance of exfoliated graphite containing MnO_2 is presented in Figure 31.

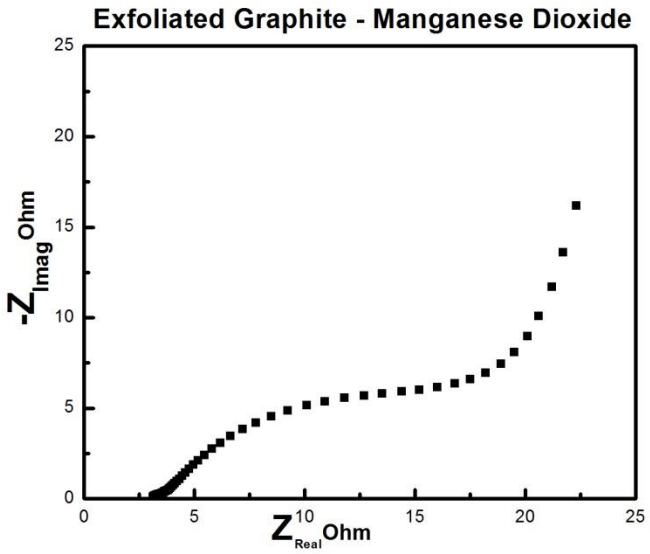

Figure 31- Impedance spectroscopy of a 1 mg electrode of an EG-MnO_2 composite.

The charge transfer resistance is increased as compared to the impedance of the pure exfoliated graphite sample. This is expected as the MnO_2 is less conductive than the Exfoliated Graphite. However, the shape of the impedance plot is more complex due to the contribution of both the exfoliated graphite and the Manganese dioxide with two different time constants. The sloped Warburg impedance tail is an indication of the charge transfer occurring in the cell during redox reactions. The impedance spectrum of the exfoliated graphite – carbon Nano-Fiber – MnO_2 is shown in Figure 32.

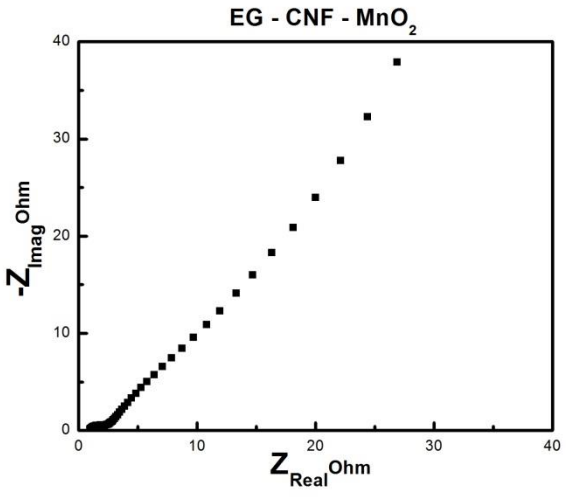

Figure 32- Impedance spectroscopy of a 1mg electrode of an EG-CNF-MnO_2 composite.

A complex impedance plot is observed with a small semicircle at the beginning of the spectrum, and a big loop almost similar to the Warburg impedance at higher frequencies. The charge transfer resistance calculated form the first semicircle is very small (<10 Ohms) indicating a fast responsive electrode desirable for high rate charging.

4.2.2 Cyclic Voltammetry

Capacitance of the various samples was obtained via cyclic voltammetry. Figure 33 shows the cyclic voltammogram of Exfoliated Graphite. The weight of the electrode was 1 mg and the electrode was cycled at a scan rate of 5 and 100 mV.S^{-1}.The total accumulated charges are obtained by integrating the area between the charging curve (positive current) and the x axis via triangulation method within the one volt range.

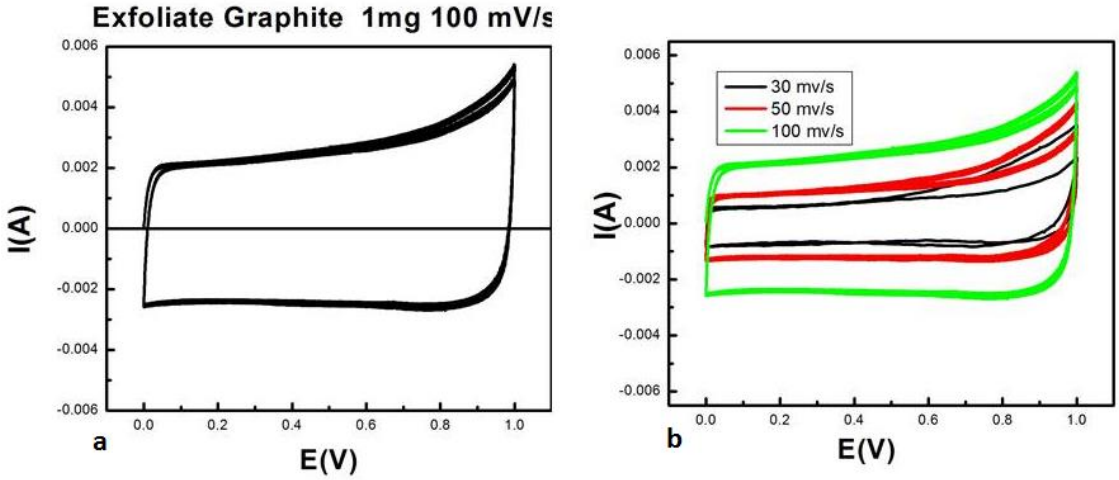

Figure 33-a) Cyclic Voltammetry of a 1 mg exfoliated graphite electrode at 100 mV/s. b) CV of exfoliated graphite at various scan rates.

The near ideal rectangular shape of the voltammogram is an indication of the activation of carbon and the creation of pores through reflux in KOH. At 5 mV.s^{-1} the electrode showed a capacitance of 40.1 F/g with a drop to almost half that value at the 100 mV.s^{-1} scan rate. The electrode showed very little drop in capacitance even after 1000 cycles.

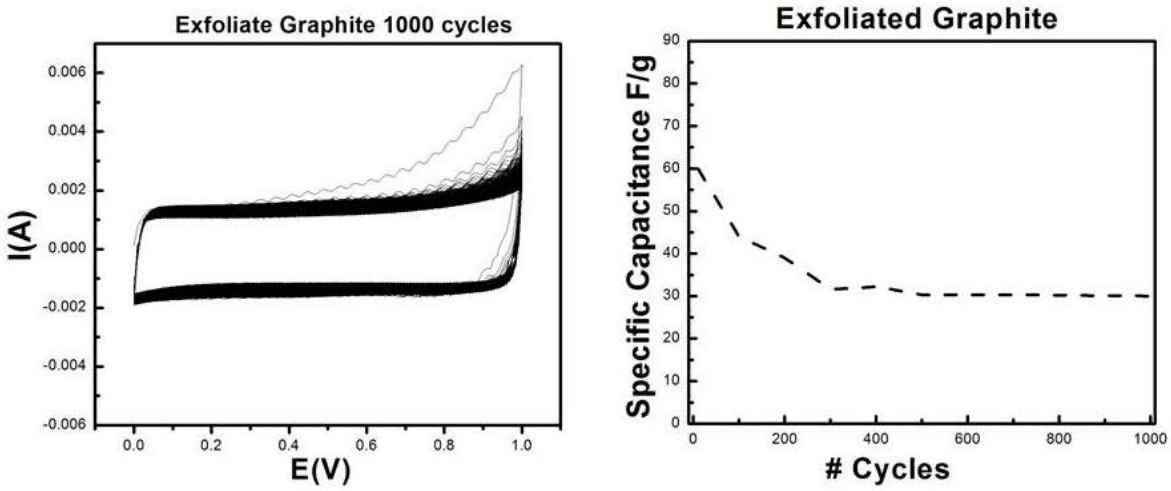

Figure 34- a) 1000 CV cycles between 0 and 1 volt. There is little sign of degradation in the shape. b) Capacity versus cycle life for an electrode containing 1 mg of EG.

After an initial drop in capacitance from 60 F/g on Cycle # 10 to finally stabilizing at around 30 F/g after the 300^{th} cycle, the Exfoliated Graphite electrode seem to exhibit stable cycling and show no further drop in capacitance. This initial high capacitance on initial cycling may be due to redox reaction of the surface groups of the graphite, which might also explain the absence of the redox peak apparent past the 10^{th} cycle at around 0.8 V, after the 300^{th} cycle.

Cyclic voltammetry of the exfoliated graphite and the MnO_2 composite is shown in Figure 35.

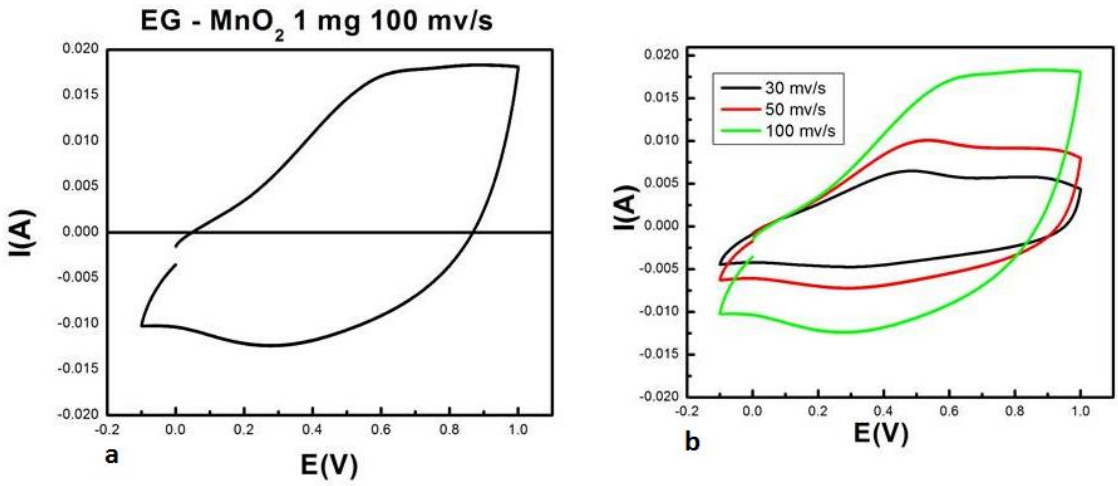

Figure 35 – a) Cyclic Voltammetry of an EG – MnO2 composite at 100 mV/s. b) CV of EG-MnO2 composite at different scan rates.

Figure 35 above shows the cyclic voltammetry of exfoliated graphite and Manganese dioxide (50:50% weight ratios) mixture. The specific capacitance was computed to be 156.9 F/g for a scan rate of 5 mV/s. The capacitance drops when the scan rate increases to 100 mV/s to 126.3 F/g which still competitive with most reported data of similar composites. The plot clearly presents a “hump” on the oxidation curve which corresponds to the pseudocapacitive behavior of MnO_2. The symmetric nearly “box-shaped” curve indicates good capacitive behavior, and high surface area as seen in the SEM of the sample (Figure 27). Figure 36 below demonstrates the stability of the sample by presenting its cycles life (1000 cycles).

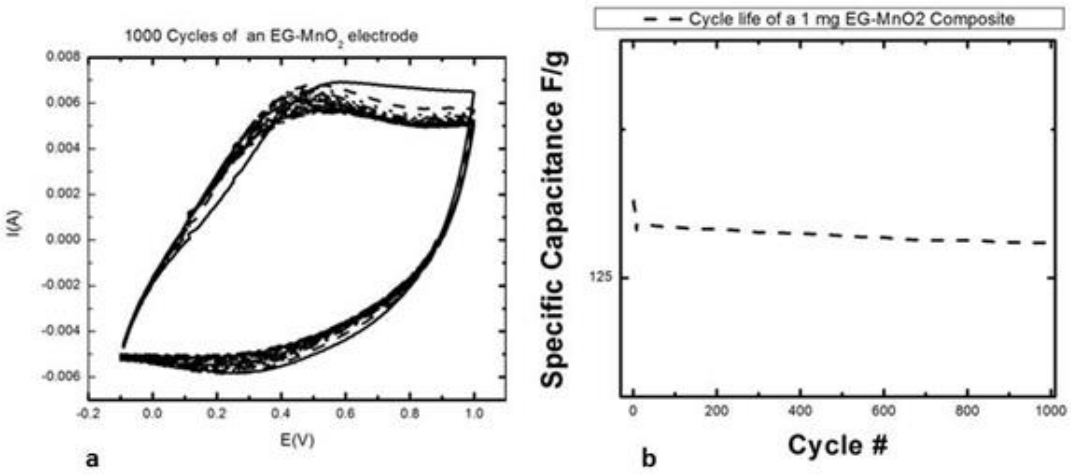

Figure 36- a) Cyclic voltammogram of 1mg electrode of EG-MnO_2 composite cycled 1000 times at 100 mv/s. b) Cycle life and capacity retention of a 1 mg electrode of Exfoliated Graphite and MnO_2 composite.

Figure 37 shows the CV of our novel EG-CNF-MnO_2 nano-composite.

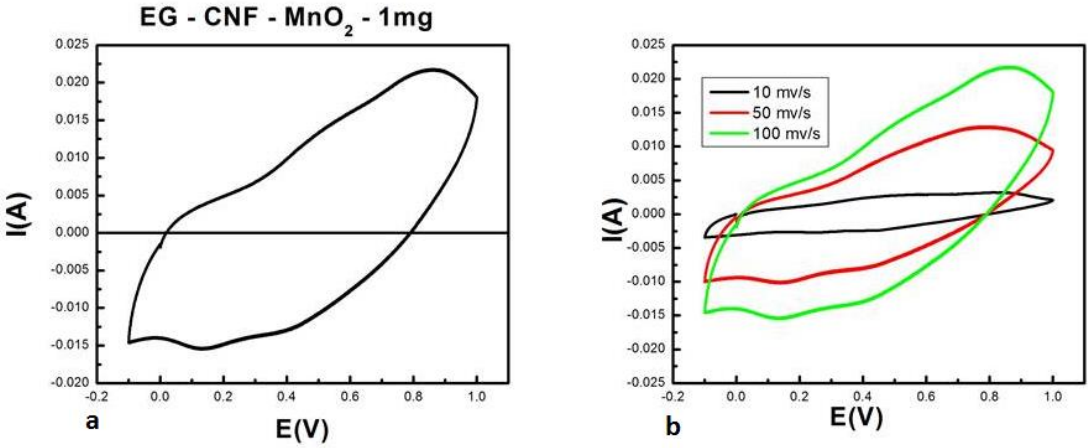

Figure 37- a) cyclic voltammogram of a 1mg EG-CNF-MnO_2 Composite, between -0.1 and 1.0 volt. b) CV of EG-CNF-MnO_2 nano-composite at different scan rates.

High specific capacitance around 200 F/g is observed for this type of composite electrodes. Figure 37 shows capacity retention of the composite. We have observed

that during extensive cycling, the electrode response becomes more capacitive like losing their redox peaks resolution with slight capacity fading. However, after 1000 cycle the capacity fading was less than 5%. It is worth noting that in figure 41; the pseudocapacitive behavior becomes noticeable around 0.5 volts, and culminated in a redox peaks typical of MnO2 according to the equation:

$$MnO_2 + e^- \rightleftharpoons MnOOH \text{ and } MnOOH + e^- \rightleftharpoons Mn(OH)_2$$

Two faradaic reactions typically happen during the oxidation of manganese on charging: near 0.43 volt, the formation of $Mn(OH)_2$ gives rise to an oxidation peak during cyclic voltammetry and again 0.6 volt when MnOOH is created. Lastly, as the applied voltage gets close to 1 volt, MnO_2 is formed on the surface of the electrode, the ionic species start to deplete from the electrolyte and the current starts to fade.

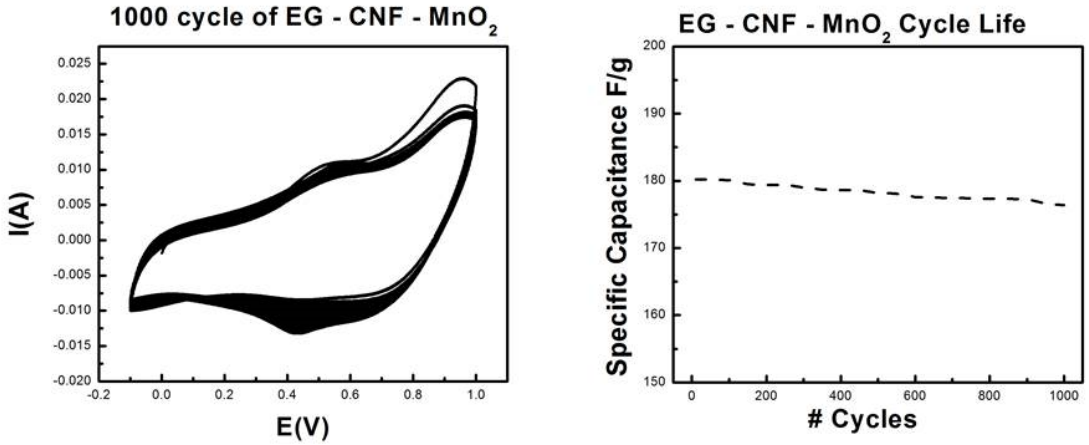

Figure 38- a) cyclic voltammogram of a 1 mg electrode of EG-CNF-MnO_2 cycled a 1000 times. b) Cycle life of a 1 mg of an EG-CNF-MnO_2 composite.

The excellent capacity retention rate of the Exfoliated Graphite (EG) – Carbon Nano-fiber (CNF) – Manganese dioxide (MnO_2) composite may be attributed to its microstructure and excellent dispersion as shown in figure 28b. The nanoscale size of MnO_2 particle will reduce is the diffusion length over which the ions in the electrolyte must transfer for charging and discharging which would enhance the conductivity of MnO_2 as presented in figure 32. The carbonaceous material (EG-CNF) act as excellent conductive channels for fast transportation of electrons to and from the surface pores.

Chapter 5

Conclusions and Future directions

The physical and chemical operation of various electrodes has been briefly mentioned such as carbons, metal oxides and carbon Nano-fiber. It is apparent that supercapacitors technology may improve by adoption of new composite, particularly the incorporation of nano sized metal oxides into high surface area supports such as graphene. The present work has shown proper selections of composite materials to provide high surface area, high conductivity, and high charge retention during cycling are crucial to further improve the capacity and cycle life of the future supercapacitors. For example, Fig. 39 compares the cyclic voltammogram of our exfoliated graphite based samples at 100 mV/s.

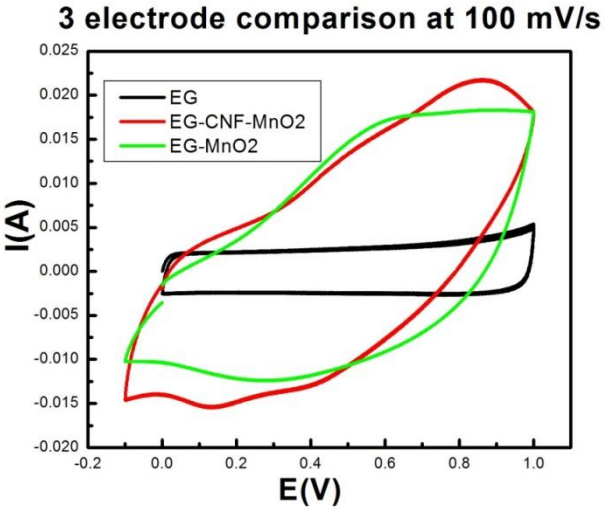

Figure 39- A comparative plot of cyclic voltammetry performance of EG, EG-MnO_2 composite, and EG-CNF-MnO_2.

Activated exfoliated graphite shows the expected shape of an EDLC with less capacitive opening (89 F/g at 5 mv/s) than samples incorporating faradaic reactions corresponding to manganese dioxide (159.7 F/g at 5 mv/s for EG-MnO_2 and 180 F/g for at 5 mv/s for EG-CNF-MnO_2). Further work is need to fine tune the loading of the material on the electrodes, as well as optimizing the different phases of the manganese dioxide, for a prime performance of our composite.

The supercapacitors are presently available with an energy density of 5–6 Whr/kg and projections of improved performance indicate that future devices could have energy densities exceeding 20-50 Whr/kg. The handful of applications described in this survey therefore represents only a small selection of the possible uses of EDLC energy storage as the technology stands today. Because of the advantages of charging efficiency, long lifetime, fast response, and wide operating temperature range, it is tempting to try and apply EDLCs to any application that requires high rate energy storage. The only current hindrance to such application is cost. This is an obstacle to be circumvented by researching lower cost material for electrodes.

Appendix

Supercapacitor sizing for HEV and EV

Since the days of the early rise of modern western civilization, global economies developed an addiction to fossil fuel which has become problematic in recent years: The rising cost of extracting crude oil and volatile geo-political situations in oil rich countries have given the electrification of transportation the boost it was looking for.

The electric vehicle started in Europe in the mid-19th century but was quickly abandoned with the discovery of the internal combustion engine, and the availability of crude oil. In the seventies, political turmoil in the Middle East placed western supplies of fuel in jeopardy and car companies scrambled for an answer. General Motors developed their EV1 model in the early nineties which was powered by an 1175 lbs. lead-acid battery pack and seated only two people. The program was quickly scrapped, and GM abandoned its efforts to electrify its vehicles until the onset of the economic downturn, when favorable consumer response, and rising environmental concern, made the electric vehicle profitable again.

Electric vehicles, despite various advancements in their technology, suffer from limited range. Some car companies thought to solve the issue with the introduction of Hybrid cars, which combines a fuel efficient internal combustion engine (ICE), with a battery pack and an electric drivetrain[90]. A hybrid power train utilizes an electric motor to supplement the power needs of the (ICE) and to capture energy via regenerative breaking. The latter is quite possibly the most remarkable advancement in vehicle

electrification in recent years, even though it is not a recent discovery[91]: Regenerative Breaking (Regen) offers the possibility of recovering the energy via a DC traction motor to operate in generator mode, some of the vehicle's kinetic energy which is normally absorbed by the brakes and turned into heat, can be reintroduced into the on-board energy and stored in Supercapacitor and reintroducing it into the on-board energy storage bank. It is a very effective approach to improving the range and energy efficiency of both EVs and HEVs[92], especially in an urban setting, where lots of braking is required such as postal fleets, inner-city buses and metro vehicles.

Another issue hindering the electrification of transportation is the size and weight of the on-board energy storage system (ESS). Range requirement tightens free space on-board the vehicle which is largely occupied by the (ESS), which in turn is rather expensive. The efficiency of an EV or HEV depends on the ability of the (ESS) to deliver large amounts of energy quickly depending on load and grade demands. Currently, Batteries are the most common (ESS) on-board most EVs and HEVs. They have superb energy density and are capable of holding a high amount of charge. On the other hand, rapid charge/discharge cycles lead to reduced performance and shortened cycle life in batteries[93].

Supercapacitors enjoy high power density, the ability to rapidly store and deliver large bursts of energy with little degradation even after thousands of cycles, and are able to store a substantial amount of charge at low voltage. Its drawbacks are a limited energy density[94].

Currently, no unique ESS system is able to meet all the requirements of EVs and HEVs. It has been postulated that in urban driving profiles, supercapacitors are ideal to capture the energy recovered from Regen, due to their long cycle life, and they are also ideal for delivering the rapid bursts of power needed to accelerate. Batteries would still be needed because of their high energy density, and combining them with a supercapacitor leads to cost effectiveness and maximize the benefits of both systems. Various topologies were introduced by researchers to combined supercapacitors with batteries and in the following is a hypothetical Battery-Supercap combo to be introduced to a modern HEV vehicle: The GM Volt.

In December 2010, GM released the Chevrolet Volt in US markets and various other international markets (under different names). It is a plug-in Hybrid electric vehicle with a lean EcoFlux 84 horse power gasoline engine and 111 Kw electric motor. On-board is 16 KWh Lithium-ion battery pack coupled with Regen granting the Volt an all-electric range of over 35 miles. Figure 51 below shows the Urban Driving Profile used to test the performance of various automobiles:

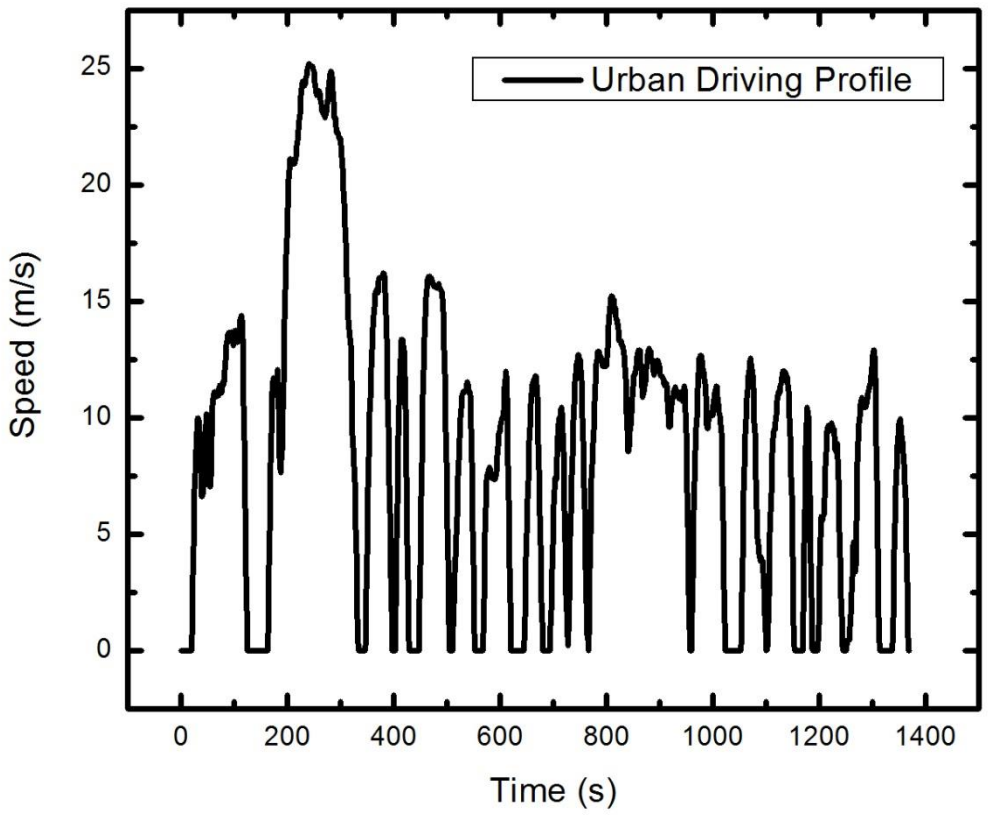

Figure 39- Urban driving profile used to test performance of EV and HEV vehicles.

The high power peak demand at the initial part of acceleration and for overcoming the road grading requires fast energy storage and release system. We are proposing a combination of Supercapacitor and the advanced battery to optimize performance and reduce the overall weight of energy storage system. In addition, usage of Supercapacitor may allow a widening of the state of charge of the battery, which leads to reducing both size and weight of the battery pack.

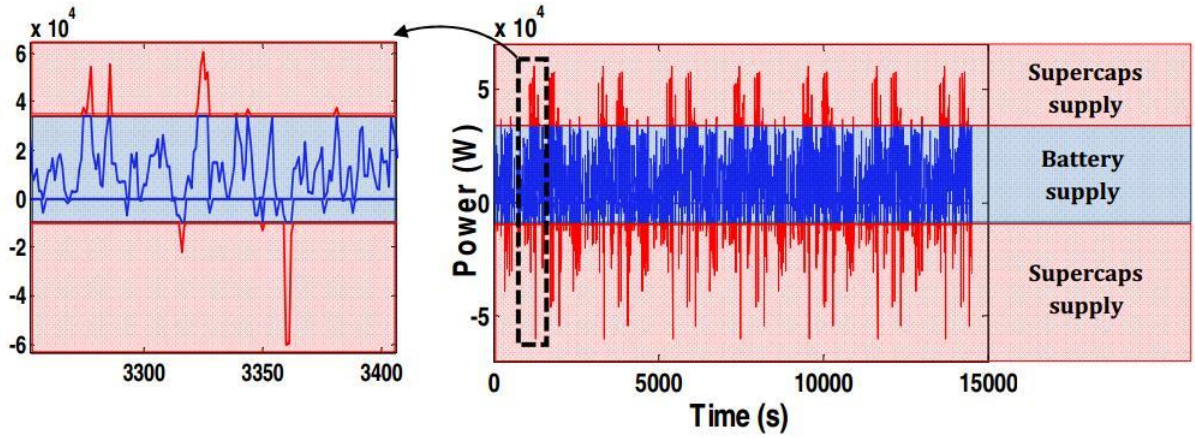

Figure 40- Repartition of the electric vehicle global power between batteries and supercapacitors[95].

In this work, we have studied the size of a Supercapacitor that can manage the storage of Regenerative Breaking energy, even when the battery is fully charged. The energy of Regen in a typical HEV is around 500 Wh. This energy is used to calculate the size of the Supercapacitor, assuming that practical energy density of the Supercapacitor is about 1/3 of its theoretical value.

During this performance profile, the theoretical value for kinetic energy available from Regenerative Braking may be computed using the equation:

$$E = \left(\frac{1}{2}\right) MV^2 \qquad (13)$$

A typical gross mass of an HEV (its curb-side mass plus the mass of two passengers) is around 2000 kg. The total Kinetic energy available from Regen was computed to be 2900000 Joules. Considering less than 100% efficiency, due the rolling frictional resistances, gravitational resistance, road grading, and aerodynamic resistance

the Regen energy of 0.8 – 1.0 KWh is generated during breaking. . This is the energy which regenerative breaking is supposed to deliver back into the battery pack. However, Regenerative Braking systems suffer from several setbacks such as mechanical frictions and heat dissipation, limiting the efficiency of Regen to less than 60%. In turn this implies that the actual total kinetic energy recovered is 0.48 – 0.6 Kwh. For our composite material (EG-CNF-MnO2) our measured capacitance of 241 F/g means that each gram of material corresponds to 0.0335 Kwh where we use the following equation to compute the energy per gram of active material:

$$\boldsymbol{E = \left(\frac{1}{2}\right) CV^2} \qquad \textbf{(14)}$$

Where C is the capacity and V the voltage.

For the purpose of this exercise, we shall make a few assumptions: We will allot 100 volt for the Supercapacitor pack and assume a loading of active material no bigger than 5 mg/cm^2.

In equation 14 above, E is the total energy capture by the Regen system (490 Wh) which will be used to compute the total weight of active material needed in the Supercapacitor pack. In practice, this theoretical value is assumed to be 1/3 of the actual energy needing for capacitor sizing, which brings the value of E from the Supercapacitor closer to 1470 Wh.

We clocked our EG-CNF-MnO_2 composite at about 200 Farad per gram or 0.066 Ah per gram for a 1 volt operating voltage. We can now compute the amount of active material needed inside the Supercapacitor bank to capture 1470 Wh of energy: 22.28 Kg for the weight of capacitor bank. This is the practical weight needed to capture the Regen energy. The theoretical value is of course limited to 7.3 Kg.

In other word, we need to distribute 7.3 Kg of active material on supercapacitor cells connected in series and parallel, each operating under one voltage to obtain the required capacitance and bring the total voltage of the pack to 100 volts.

Considering that current on board energy storage packs, are limited to about 50 % state of charge for various safety and practical operating conditions, designating a Supercapacitor pack made of our EG-CNF-MnO2 composite as power assist and regenerative breaking energy capture device, would improve the efficiency of the battery pack by over 20% by allowing a widening of the state of charge. This widening of battery SOC from 50% to 70% will justify the excess weight of supercapacitor, in addition to the overall improvement in vehicle performance.

References

1. S. Shafiee and E. Topal, Energy Policy **37** (1), 181-189 (2009).
2. M. Asif and T. Muneer, Renewable and Sustainable Energy Reviews **11** (7), 1388-1413 (2007).
3. J. P. Dorian, H. T. Franssen and D. R. Simbeck, Energy Policy **34** (15), 1984-1991 (2006).
4. P. J. Hall, Energy Policy **36** (12), 4363-4367 (2008).
5. F. Gonzalez, in *IDTechEX* (2014), Vol. 2014.
6. G. Kable, edited by Autocar (Web, 2014), Vol. 2014.
7. K. A. C. Shuai Lu, Mehdi Ferdowsi, IEEE **56** (4), 1516 - 1523 (2007).
8. Y. B. S. Pay, in *IEEE Bologna PowerTech Conference* (Bologna, Italy, 2003).
9. J. Van Mierlo, P. Van den Bossche and G. Maggetto, Journal of Power Sources **128** (1), 76-89 (2004).
10. J. Moreno, M. E. Ortuzar and J. W. Dixon, Industrial Electronics, IEEE Transactions on **53** (2), 614-623 (2006).
11. Y. Wang, J. Chen, J. Cao, Y. Liu, Y. Zhou, J.-H. Ouyang and D. Jia, Journal of Power Sources (0), 87-96 (2009).
12. Q. Wu, Y. Xu, Z. Yao, A. Liu and G. Shi, ACS Nano **4** (4), 1963-1970 (2010).
13. J. Rantala, J. Hännikäinen and J. Vanhala, Pers Ubiquit Comput **15** (1), 85-96 (2011).
14. M. S. Halper, (Mitre Corporation, Mitre.org, 2006).
15. M. Mastragostino, Arbizzani, C., Soavi, F., Journal Of Power Sources **98**, 812 - 815 (2001).
16. B. E. Conway, *Electrochemical Supercapacitors: Scientific Fundamentals and Technological Applications.* (Springer, New York, 1999).
17. Q. Wang, Z. H. Wen and J. H. Li, Advanced Functional Materials **16** (16), 2141-2146 (2006).
18. D. Chen, L. Tang and J. Li, Chemical Society Reviews **39** (8), 3157-3180 (2010).
19. M. Winter and R. Brodd, Chemical Reviews **104** (10), 4245-4269 (2004).
20. P. Sharma and T. S. Bhatti, Energy Conversion and Management **51** (12), 2901-2912 (2010).
21. V. S. Bagotsky, in *Fundamentals of Electrochemistry* (John Wiley & Sons, Inc., 2005), pp. 369-377.
22. E. Frackowiak and F. Béguin, Carbon **39** (6), 937-950 (2001).
23. M. Inagaki, H. Konno and O. Tanaike, Journal of Power Sources **195** (24), 7880-7903 (2010).
24. J. i. Hayashi, A. Kazehaya, K. Muroyama and A. P. Watkinson, Carbon **38** (13), 1873-1878 (2000).
25. J. Wang and S. Kaskel, Journal of Materials Chemistry **22** (45), 23710-23725 (2012).
26. D. Qu and H. Shi, Journal of Power Sources **74** (1), 99-107 (1998).
27. C. Merino, P. Soto, E. Vilaplana-Ortego, J. M. Gomez de Salazar, F. Pico and J. M. Rojo, Carbon **43** (3), 551-557 (2005).
28. G. L. A.B. Fuertesb, T.A. Centenob, E. Frackowiak, Electrochimica Acta **50** (27), 2799–2805 (2005).
29. E. F. Cathie Vix-Guterla, Krzysztof Jurewiczb, Marcin Friebeb, d, Julien Parmentierc, François Béguind, Carbon **43** (6), 1293–1302 (2005).

30. S. S. C. Vix-Guterla, K. Jurewiczb, E. Frackowiakb, M. Redaa, J. Parmentierc, J. Patarinc, F. Beguin, Materials Science and Engineering B **108** (1-2), 148-155 (2004).
31. G. Tourillon, L. Pontonnier, J. P. Levy and V. Langlais, Electrochemical and Solid-State Letters **3** (1), 20-23 (2000).
32. A. L. M. Reddy and S. Ramaprabhu, The Journal of Physical Chemistry C **111** (21), 7727-7734 (2007).
33. R. H. Baughman, A. A. Zakhidov and W. A. de Heer, Science **297** (5582), 787-792 (2002).
34. T. W. Odom, J.-L. Huang and C. M. Lieber, Annals of the New York Academy of Sciences **960** (1), 203-215 (2002).
35. E. Frackowiak, K. Metenier, V. Bertagna and F. Beguin, Applied Physics Letters **77** (15), 2421-2423 (2000).
36. K. Koziol, J. Vilatela, A. Moisala, M. Motta, P. Cunniff, M. Sennett and A. Windle, Science **318** (5858), 1892-1895 (2007).
37. T. Hasobe, S. Fukuzumi and P. V. Kamat, Angewandte Chemie **118** (5), 769-773 (2006).
38. M. Endo, Y. A. Kim, T. Hayashi, Y. Fukai, K. Oshida, M. Terrones, T. Yanagisawa, S. Higaki and M. S. Dresselhaus, Applied Physics Letters **80** (7), 1267-1269 (2002).
39. C. Kim, Y. J. Kim, Y. A. Kim, T. Yanagisawa, K. C. Park, M. Endo and M. S. Dresselhaus, Journal of Applied Physics **96** (10), 5903-5905 (2004).
40. I. Y. Jang, H. Ogata, K. C. Park, S. H. Lee, J. S. Park, Y. C. Jung, Y. J. Kim, Y. A. Kim and M. Endo, The Journal of Physical Chemistry Letters **1** (14), 2099-2103 (2010).
41. A. K. Geim, Novoselov, K.S., Nature Materials **6** (3), 183 - 191 (2007).
42. M. D. Stoller, S. Park, Y. Zhu, J. An and R. S. Ruoff, Nano Letters **8** (10), 3498-3502 (2008).
43. J. Xia, Chen, F., Li, J., Tao, N., Nature Nano **4** (8), 505 - 509 (2009).
44. Y. Wang, Z. Shi, Y. Huang, Y. Ma, C. Wang, M. Chen and Y. Chen, The Journal of Physical Chemistry C **113** (30), 13103-13107 (2009).
45. J. T. Qian Cheng, Jun Ma, Han Zhang, Norio Shinya, Lu-Chang Qin, Carbon **49**, 2 9 1 7 – 2 9 2 5 (2011).
46. D. A. C. Brownson, D. K. Kampouris and C. E. Banks, Journal of Power Sources **196** (11), 4873-4885 (2011).
47. M. F. El-Kady, V. Strong, S. Dubin and R. B. Kaner, Science **335** (6074), 1326-1330 (2012).
48. R. L. L. João Paulo C. Trigueiro, Glaura G. Silva, Journal of Power Sources **256**, 264-273 (2014).
49. C. Liu, Z. Yu, D. Neff, A. Zhamu and B. Z. Jang, Nano Letters **10** (12), 4863-4868 (2010).
50. S. R. C. Vivekchand, C. Rout, K. S. Subrahmanyam, A. Govindaraj and C. N. R. Rao, J Chem Sci **120** (1), 9-13 (2008).
51. Y. Zhu, S. Murali, M. D. Stoller, K. J. Ganesh, W. Cai, P. J. Ferreira, A. Pirkle, R. M. Wallace, K. A. Cychosz, M. Thommes, D. Su, E. A. Stach and R. S. Ruoff, Science **332** (6037), 1537-1541 (2011).
52. V. C. Tung, M. J. Allen, Y. Yang and R. B. Kaner, Nat Nano **4** (1), 25-29 (2009).
53. O. domain, (Wikipedia, Wikicummons, 2011), Vol. 2014.
54. B. E. Conway, Journal of The Electrochemical Society **138** (6), 1539-1548 (1991).
55. B. E. Conway, Birss, V., Birss, V., Journal of Power Sources **66** (1-2), 1 - 14 (1997).
56. S. Sarangapani, B. V. Tilak and C. P. Chen, Journal of The Electrochemical Society **143** (11), 3791-3799 (1996).

57. J.-K. Chang and W.-T. Tsai, Journal of The Electrochemical Society **150** (10), A1333-A1338 (2003).
58. E. Raymundo-Piñero, V. Khomenko, E. Frackowiak and F. Béguin, Journal of The Electrochemical Society **152** (1), A229-A235 (2005).
59. J. Z. S. Chen, X. Wu, Q. Han, X. Wang, ACS nano **4** (5), 2822–2830 (2010).
60. R. G. R. Ravinder N. Reddy, Journal Of Power Sources **132** (1 - 2), 315–320 (2003).
61. C. Arbizzani, Mastragostino, M., Soavi, F, Journal of Power Sources **100** (1 - 2), 164 - 170 (2001).
62. G. A. Snook, P. Kao and A. S. Best, Journal of Power Sources **196** (1), 1-12 (2011).
63. R. C. Johnson, in *EE times* (EDN network, 2011).
64. A. Burke, Journal Of Power Sources **91**, 37 - 50 (2000).
65. *New Materials for Sustainable Energy and Development : Supercapacitors*. (Wiley, Somerset, NJ, USA, 2013).
66. Y.-g. Wang, L. Yu and Y.-y. Xia, Journal of The Electrochemical Society **153** (4), A743-A748 (2006).
67. F. Béguin, V. Presser, A. Balducci and E. Frackowiak, Advanced Materials **26** (14), 2219-2251 (2014).
68. V. Khomenko, E. Raymundo-Piñero, E. Frackowiak and F. Béguin, Applied Physics A **82** (4), 567-573 (2006).
69. Q. Gao, L. Demarconnay, E. Raymundo-Pinero and F. Beguin, Energy & Environmental Science **5** (11), 9611-9617 (2012).
70. M. Galiński, A. Lewandowski and I. Stępniak, Electrochimica Acta **51** (26), 5567-5580 (2006).
71. M. Ue, Journal of The Electrochemical Society **141** (12), 3336-3342 (1994).
72. P. Azaïs, L. Duclaux, P. Florian, D. Massiot, M.-A. Lillo-Rodenas, A. Linares-Solano, J.-P. Peres, C. Jehoulet and F. Béguin, Journal of Power Sources **171** (2), 1046-1053 (2007).
73. J. Chen, B. Yao, C. Li and G. Shi, Carbon **64** (0), 225-229 (2013).
74. Y. Zhu, S. Murali, M. D. Stoller, A. Velamakanni, R. D. Piner and R. S. Ruoff, Carbon **48** (7), 2118-2122 (2010).
75. S. Pei and H.-M. Cheng, Carbon **50** (9), 3210-3228 (2012).
76. D. D. L. Chung, J Mater Sci **22** (12), 4190-4198 (1987).
77. M. Toyoda, J. Aizawa and M. Inagaki, Desalination **115** (2), 199-201 (1998).
78. M. Inagaki, R. Tashiro, Y.-i. Washino and M. Toyoda, Journal of Physics and Chemistry of Solids **65** (2–3), 133-137 (2004).
79. H. J.R, H.E., HALL, *Solid State Physics*. (John Wiley & Sons, Manchester, England).
80. A. S. Judith, Physics Education **17** (3), 111 (1982).
81. L. Athouël, F. Moser, R. Dugas, O. Crosnier, D. Bélanger and T. Brousse, The Journal of Physical Chemistry C **112** (18), 7270-7277 (2008).
82. M. DD, Electrochim. Acta **51**, 1376 (2006).
83. A. Di Fabio, A. Giorgi, M. Mastragostino and F. Soavi Journal of The Electrochemical Society **148** (8), A845-A850 (2001).
84. G. Instruments, (2010).
85. in *Electrochemical Supercapacitors for Energy Storage and Delivery* (CRC Press, 2013), pp. 277-316.
86. J. Wang, *Analytical Electrochemistry*. (John Wiley and Sons, 2000).

87. M. Fang, K. Wang, H. Lu, Y. Yang and S. Nutt, Journal of Materials Chemistry **19** (38), 7098-7105 (2009).
88. H. Fujimoto, Carbon **41** (8), 1585-1592 (2003).
89. Z. Q. Li, C. J. Lu, Z. P. Xia, Y. Zhou and Z. Luo, Carbon **45** (8), 1686-1695 (2007).
90. A. Chu and P. Braatz, Journal of Power Sources **112** (1), 236-246 (2002).
91. C. J. Paulson, (Google Patents, 1908).
92. J. Erjavec, (Cengage Learning, Inc.), pp. 96-97.
93. S. M. Lukic, J. Cao, R. C. Bansal, F. Rodriguez and A. Emadi, Industrial Electronics, IEEE Transactions on **55** (6), 2258-2267 (2008).
94. A. Khaligh and L. Zhihao, Vehicular Technology, IEEE Transactions on **59** (6), 2806-2814 (2010).
95. R. Sadoun, N. Rizoug, P. Bartholomeus, B. Barbedette and P. Le Moigne, presented at the Vehicle Power and Propulsion Conference (VPPC), 2011 IEEE, 2011 (unpublished).

ABSTRACT

NOVEL NANO COMPOSITE MATERIAL FOR SUPERCAPACITOR APPLICATIONS

by

WISSAM FAWAZ

August 2014

Advisor: Dr. Gholam-Abbas Nazri

Major: Physics

Degree: Master of Science

With the rapid development of electric-based transportation and introduction of various hybrids, plug-in and full electric vehicles, there is an urgent need to develop a high power energy storage system to complement the high energy density batteries, to extend the range and life of HEVs and EVs. In this work, we have developed and optimized a unique composite material that can serve as electrode materials for high power supercapacitor for various applications. The material is prepared form high surface area graphene–like carbon made from exfoliated graphite flakes through thermal shock process. The expanded graphite then is mixed with functionalized stacked cone carbon nano-fiber. The mixture was impregnated with nano size manganese oxide, MnO_2, to further enhance the energy storage density and the high rate capability of the composite material. The formulation of our composite mixture contains, [(graphene) –

(carbon nano-fiber), (MnO_2)]. The optimized composite mixture was impregnated into metal foam that served as a current collector in an electrochemical cell.

The X-ray diffraction of the composite has shown formation mixed phases of MnO_2, and SEM results indicate uniform deposition of oxide on graphene-like carbon and on carbon nano-fibers. The electrochemical performance of the composite was tested for its energy storage capacity (F/g) and for its high rate capability using cyclic voltammetry. The stability of the composite was also tested during multiple charge-discharge cycles. The composite electrode provides very good charge storage capacity (~ 200 F/g), with high charge-discharge cycling stability over 1000 deep cycles. Further optimization and scale – up of the composite material is in progress.

AUTOBROGRAPHICAL STATEMENT

I, Wissam Fawaz, was born in Beirut Lebanon, on August 3. After the Israeli invasion a year later the family moved to France, and upon graduation with a baccalaureate of science, I joined the Lebanese University's faculty of Science for a year as well as the Political Science department before moving to the Wayne State University.

In Detroit, I finished my undergraduate studies with a major in Mathematics and a minor in Physics. The seed of scientific discovery was planted and I decided to go onwards in graduate studies in Physics and Engineering.